Review

N.J. Henry Holroyd*, Timothy L. Burnett, John J. Lewandowski and Geoffrey M. Scamans

Crack initiation during environment-induced cracking of metals: current status

https://doi.org/10.1515/corrrev-2024-0034
Received March 5, 2024; accepted April 9, 2024;
published online July 5, 2024

Abstract: Environment-induced cracking (EIC) research spanning the last 80 years for ferrous and non-ferrous metals in aqueous environments at ambient and elevated temperatures has concentrated on crack propagation. Studies clearly reveal EIC involves two differentiable processes, one controlling initiation and the other propagation. Utilization of advanced high-resolution electron microscopyover the last 20 years has enabled more focused studies of crack initiation for stainless steel and nickel-based alloys at elevated temperatures exposed to environments associated with the nuclear industry. More recently, when coupled with advanced in-situ experimental techniques such as time-lapse X-ray computed 3D-tomography, progress has also been made for aluminum alloys suffering EIC at ambient temperatures. Conventional wisdom states that chemical processes are typically ratecontrolling during EIC initiation. Additionally, experimental evidence based on primary creep exhaustion ahead of the introduction of an aggressive environment indicates that time-dependent mechanically-driven local microstructural strain accommodation processes (resembling creep-like behavior) often play an important role for many metals, even for temperatures as low as 40 % of their melting points (0.4 T_m). EIC studies reveal initial surface conditions and their associated immediate sub-surface alloy microstructures generated during creation (i.e. disturbed layers) can dictate whether or not EIC initiation occurs under mechanical loading conditions otherwise sufficient to enable initiation and growth. The plethora of quantitative experimental techniques now available to researchers should enable significant advances towards understanding EIC initiation.

Keywords: crack initiation; metallic alloys; environmentinduced cracking; crack arrest

*Corresponding author: N.J. Henry Holroyd, Department of Materials Science and Engineering, Case Western Reserve University, Cleveland, OH,
USA; and The Department of Materials, The University of Manchester, Manchester, M13 9PL, UK, E-mail: henry.holroyd@luxfer.com
Timothy L. Burnett, The Department of Materials, The University of Manchester, Manchester, M13 9PL, UK
John J. Lewandowski, Department of Materials Science and Engineering, Case Western Reserve University, Cleveland, OH, USA
Geoffrey M. Scamans, Innoval Technology Ltd, Banbury, OX16 1TQ, UK; and BCAST, Brunel University, Uxbridge, Middlesex, UBB 3PH, UK

1 Introduction

Chapter 1, the first chapter of a recently published book that provides an overview of environment induced cracking EIC in metallic alloys, 'Mechanics-Microstructure-Corrosion' Coupling, Blanc and Aubert (2019) confirms that research in this field has focused on crack propagation, paying little attention to the initiation process, which typically originates from an alloys surface layers that often have different microstructure and sometimes different composition compared to the bulk alloy (Combrade 2019). In view of this anomaly, we have carried out a review of the literature on initiation processes for EIC in both ferrous and non-ferrous alloys exposed to aqueous environments at both ambient and elevated temperatures.

Efforts to characterize EIC initiation started during the mid-1950s, continued through the late-1970s (Bakish and Robertson 1956a,b; Eckel 1962; Kohl 1967; Louthan 1965; Pickering and Swann 1963; Silcock and Swann 1977; Smith and Staehle 1967; Sugimoto et al. 1978; Swann 1963; Szklarska-Smialowska and Gust 1979; Tromans and Nutting

1962), but decreased with the introduction of pre-cracked fracture mechanics type test specimens (Brown and Beachem 1965; Novak and Wolfe 1970) and the increased use of slow strain rate testing (Henthorne 2016; Ugiansky and Payer 1979), which modify aspects of the EIC initiation process. Activity continued through the 1980s for non-ferrous (Cassagne et al. 1986; Sieradzki et al. 1987) with a resurgence for ferrous alloys (pipeline, high-strength and stainless steels) beginning during the late-1980s (Blanc et al. 2019; Fairweather et al. 2008; Isaacs 1988; Jones and Simonen 1994; Locci et al. 1987; Maiya 1989; Parkins 1988; Scenini et al. 2019), supported by an increased use of high-resolution electron microscopy (Arioka et al. 2007; Lozano-Perez et al. 2014; Staehle 2010) and in-situ experimentation. Increased activities on nickel-based alloys (Bruemmer and Thomas 2008; Le Hong 2001; Moss and Was 2017; Zhai et al. 2017a,b) and austenitic stainless steels (Fairweather et al. 2008; Kamaya and Takumi 2007; LozanoPerez et al. 2014) were conducted over a decade later in studies at elevated temperatures and environments associated with the nuclear industry, which has continued to date (Fujii et al. 2019; Kuang and Was 2000; Shen et al. 2022; Volpe et al. 2020).

For over 80 years it's been known EIC involves two processes; one controlling initiation and the other propagation (Eckel 1962; Forty 1959; Harwood 1956, 1960; Hines 1961; Hoar and Hines 1956a,b; Lee et al. 1988; Smialowski and Kostanski 1979; Sugimoto et al. 1978).

The lack of research focus on the initiation phase was noted by Hirth (1977) who concluded in his summary of issues arising during a major EIC International Conference, NACE-5 Stress Corrosion Cracking and Hydrogen Embrittlement of Iron based alloys held in France in 1973 that: "It seems that crack initiation is more or less being neglected in comparison to measurements of crack propagation as a function of stress intensity, whereas the incubation time could be a significant fraction of the life in many cases of cracking". More recent publications have confirmed this observation stating that

"On the crack initiation and early-stage crack growth in Stage 1: This is a stage that is less studied and presents many contradictions", Chen (2017) and that "Crack initiation is the least explored stage and is not clearly defined", Hojna (2021).

Our literature review has found that for all metallic alloy/environment systems known to suffer EIC (see subset provided in Table 1), strain-rate/time dependent metallurgical processes influence the rate-controlling processes during precursor and initiation phases of EIC, irrespective of tests being conducted at temperatures below 0.4 of the melting point (T_m) of an alloy. These findings challenge the current view that chemically-driven processes control the earliest stages of EIC initiation at ambient temperatures that become increasingly less dominant at elevated temperatures where local creep-related processes such as grain boundary cavitation and/or a crystalline ordering become important (Ahn 2021; Arioka 2015, 2020; Shen et al. 2022).

Efforts to quantitatively separate the initiation and propagation stages of EIC have only partially succeeded, although the experimental evidence obtained for various metal/aqueous environments supports different ratedetermining processes controlling crack initiation and crack propagation as the determined activation energies are significantly higher for crack initiation (> 100 kJ/mol) than propagation (< 100 kJ/mol), Table 1.

The comparison of published EIC initiation data is made more complicated by the inter-changeable use of the terms induction, incubation and initiation and the wide range of resolution limits for the experimental techniques used to detect EIC initiation, as shown in Table 2, often yielding different results for a given set of experimental conditions and the absence of an accepted definition for EIC initiation that has prevailed since the 1960s (Eckel
1962).

Table ?: A sub-set of EIC susceptible metal/environment systems with experimental evidence for different processes controlling of initiation and propagation rates.

Alloy	Environment	EIC test method	EIC detection method	Temperature (°C)	Apparent activation energy, E_a (kJ/mol)		References
					Initiation	Propagation	
α-Brass (??Cu–??Cu) annealed	$Cu(NH_3)_n^{2+}$ ($CuCO_3$ in NH_3) at FCP –??? mV (SCE)	Constant load ?? MPa (?? % YS)	Visual and metallographic evaluation of interrupted temperature tests (intergranular)	Room			Sircar and Narsaria (????)
Al–?Zn–?.? Mg peak aged	Distilled water	Constant load ??–??? MPa (YS = ??? MPa)	In-situ high-resolution op- ?–??°C tical (intergranular)		???		?? Abe et al. (????)

Al–□.□Zn–□.□ Mg slightly overaged	□.□M NaCl + □ wt% $K_□CrO_□$, pH = □	Fixed displacement (smooth notch K = □□ $MNm^{-□/□}$)	Load relaxation (intergranular)	□□–□□□°C □–□□°C	□□□ ± □□ □□□ ± □	– Pathania □□□□; □□ Pathania and Tromans □□□□
AZ□□B magnesium alloy	□.□M NaCl + □□ g/L $K_□CrO_□$,	Constant load	Extension – time (±□□ μm), □□°C FCP – time (±□ mV SCE at RT)			Logan (□□□□)
Austenitic stainless steel □□.□C r–□.□Ni–□.□□Mo	□□ wt% $MgCl_□$ (~□□□°C)	Constant load □□□ MPa (> YS, □□ % UTS)	Extension – time (±□□ μm)	FCP: □□□–□□□°C □□□–□□□°C (FCP) –□□□ mV (SCE): □□–□□□°C □□□–□□□°C	□□ □□ □□ □□	□□ Kohl (□□□□) □□ □□ □□

Table □: (continued)

Alloy	Environment	EIC test method	EIC detection method	Temperature (°C)	Apparent activation energy, E_a (kJ/mol)		References
					Initiation	Propagation	
Austenitic stainless steel	□□ wt% $MgCl_□$ (□□□°C)	Constant load □□□–□□□ MPa	Extension – time (±□□ μm), FCP – time (±□ mV SCE at RT)	□□□°C			Desjardins et al. (□□□□)
Austenitic stainless steel	□□ & □□ wt% $MgCl_□$(□□□°C)	Constant load (□□, □□ & □□ % UTS)	Extension – time (±□□ μm), FCP – time (±□ mV SCE at RT)	□□□°C			Bleckmann and Zitter (□□□□)
□□.□Cr–□.□Ni annealed	□□.□ wt% $MgCl_□$ (□□□°C)	Constant load □□□ MPa (□□ % YS)	Extension – time (±□□ μm), FCP time (±□ mV SCE at RT) (transgranular)	□□□–□□□°C	□□□ ± □□	□□ ± □	Sugimoto et al. (□□□□)
Alloy □□□□□Ni–□□Cr–□Fe millannealed	Hydrogenated water/steam	Reverse U-bend	>□□ % test optical crack detection, (□□–□□□ magnification) > □ mm detected (intergranular)	□□□–□□□°C	□□□	–	Economy et al. (□□□□)
		Constant load	In-situ potential-drop (intergranular)		□□□ ± □□		Richey et al. (□□□□)
					□□□ ± □□		Etien et al. (□□□□)
		Fixed strain via SSRT alloy □□□ (□ × $□□_{-□}$/s), alloy □□□ (□ × □□$^{-□}$/s) Tensile bar, □ mm dia., □□.□ mm GL	Metallography (x□□□□) (intergranular)	□□□–□□□°C	□□□ ± □□ (□ % strain) □□□ ± □□ (□ % strain)		Moss and Was (□□□□) Moss and Was (□□□□)
Alloy □□□□□Ni–□□.□Cr–□□Fe millannealed				□□□–□□□°C	□□ ± □□		Moss and Was (□□□□)

Table □: Experimental methods used to detect EIC initiation in various metallic alloy/environment systems.

EIC initiation detection method	Initial depth of event detected (μm)	Example (reference)

Ex-situ optical ± metallography	~□□ μm	□□-□ stainless steel in boiling $MgCl_{□}$ (Eckel □□□□; Sugimoto et al. □□□□)
In-situ optical ± time-lapse video	(xx_{a}–□□□$_{b}$) μm	Al–Zn–Mg–Cu alloy □□°C water vapour (Euesden et al. □□□□)
		□□-□ stainless steel intermittent boiling $MgCl_{□}$ (Kirk et al. □□□□)
In-situ X-ray tomography	~□ μm	AA□□□□ humid air, RT (Gudla et al. □□□□)
Ex-situ surface replica's (acetates)	□□ μm	Al–Zn–Mg–Cu alloy in □.□M NaCl + potassium dichromate solution (pH □.□) at RT (Hilfrich □□□□)
Electrode potential during straining	>□□□ μm	□□-□ stainless steel in boiling $MgCl_{□}$ (Bleckmann and Zitter □□□□; Desjardins et al. □□□□; Petit and Desjardins □□□□; Hoar and Hines □□□□, □□□□a; Sugimoto et al. □□□□)
Resistance-time (potential drop)	~□□□ μm	Al–Zn–Mg–Cu (McHardy and Hollingsworth □□□□) Pipeline steel (Wang and Atrens □□□□) Nickel □□□ (Anderson and Chou □□□□; Zhia et al. □□□□)
Elongation-time, constant-load[a]	>□□□–□,□□□ μm	AZ□□B magnesium alloy in NaCl/$K_{□}CrO_{□}$ at RT (Logan □□□□) □□-□ stainless steel in boiling $MgCl_{□}$ (Brauns and Ternes □□□□; Kohl □□□□; Sugimoto et al. □□□□)
Load relaxation, constantdisplacement[a]	>□□□–□,□□□ μm	Stainless steel in water at □□□°C (Wilde □□□□)
Acoustic emission	~□ mm	□□□ stainless steel simulated BWR water □□□°C (Hickling et al. □□□□) □□□ stainless steel boiling □.□M NaCl, pH □.□ (Anita et al. □□□□)
Electrochemical noise	□□□–□□□ μm's	Sensitized □□□ stainless steel water (□□°C) + □□□ ppm NaCl or □□ ppm sodium thiosulphate (Jones et al. □□□□)
Laser light 'speckle'	>□□□ μm's	AA□□□□-T□□.□M NaCl, RT (Shi et al. □□□□)
Scanning atomic force microscopy	A few μm's	Al–Zn–Mg in lab air, RT (Komai et al. □□□□)

[a] [b] Sensitive to specimen dimensions. (Authors: give explanation).

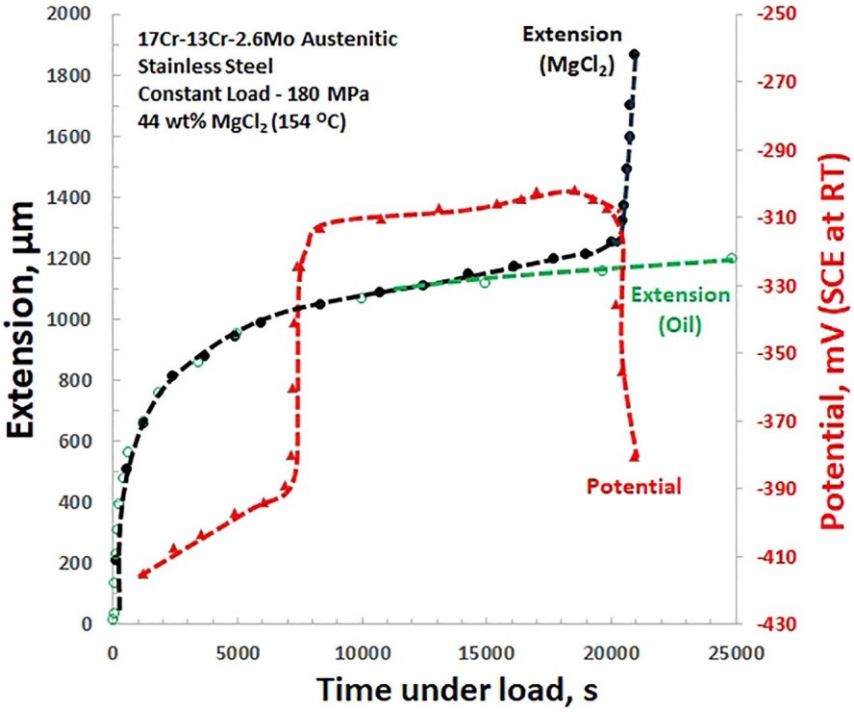

Figure 1: Gauge length extension and electrochemical potential as a function of time for an annealed austenitic stainless steel wire exposed to boiling 44 wt% $MgCl_2$ and an inert environment (oil) under a constant load of 180 MPa. The extension and electrochemical potential are shown as a linear function of time under load. Date taken from Desjardins et al. (1980).

An example of different initiation time predictions for a given set of experimental conditions is provided by the EIC data reported by Desjardins et al. (1980) for 18Cr–10Ni austenitic stainless alloys in boiling 44 wt% $MgCl_2$ (~154 ˚C) under constant load testing. Metallographic examination of interrupted constant load tests revealed that EIC microcracks initiated after the sudden electrochemical potential increase but ahead of divergence of the extension-time behavior from that obtained in an inert environment, Figure 1.

Had interrupted testing and off-line metallography not been used to determine when EIC had initiated, three different estimates of crack initiation may be based on: a) the potential-time behavior, b) the initial observation of divergence between extension behavior in an inert and aggressive environment or c) the onset of rapid extension.

Until recently our understanding of the 'how, when and if' for intergranular or transgranular EIC initiation and any subsequent transition to stable crack propagation has been restricted by our inability to consistently reproduce EIC initiation processes in the laboratory representative of service-related mechanical and environmental conditions (Colwell et al. 2008) and a limited availability of suitable high resolution experimental characterization techniques.

Detailed in-situ based studies, including use of state-ofthe-art electron microscopy and 3D X-ray computed tomography to characterize EIC initiation are now available for a range of material/environment combinations including the latest generation of high-strength Al–Zn–Mg–Cu alloys exposed to water vapor at ambient temperature (Burnett et al. 2023; Euesden et al. 2023).

2 EIC initiation process

EIC initiation is a complex phenomenon involving several process steps, before, during and after the appearance of initial micro-cracks, which may or may not subsequently undergo self-sustained EIC propagation to become deep cracks.

Our analysis shows that the EIC of metallic alloys involves three process steps, as first suggested in the 1960s for high-strength aluminum alloys in aqueous saline solutions at room temperature (Hunter and Fickle 1968; McHardy and Hollingsworth 1966). As shown in Figure 2A, this was confirmed during the 1970s for austenitic stainless steels in boiling concentrated $MgCl_2$ solution, Bleckmann and Zitter (1974) and as shown in Figure 2B and reported for nickel 600 type alloys in high temperature water (~360 °C) (Boursier et al. 1992, 1995; Le Hong 2001; Rios et al. 1995).

The three steps are shown in Figure 2B, as: 1) Incubation (Precursor), 2) Micro-crack initiation and early growth and 3) High growth rate EIC after the local mechanical driving force exceeds a minimum, such as a threshold stress intensity factor, K_{IEIC}. These process steps involve an array of overlapping phenomena, depicted in Figure 3, that is based

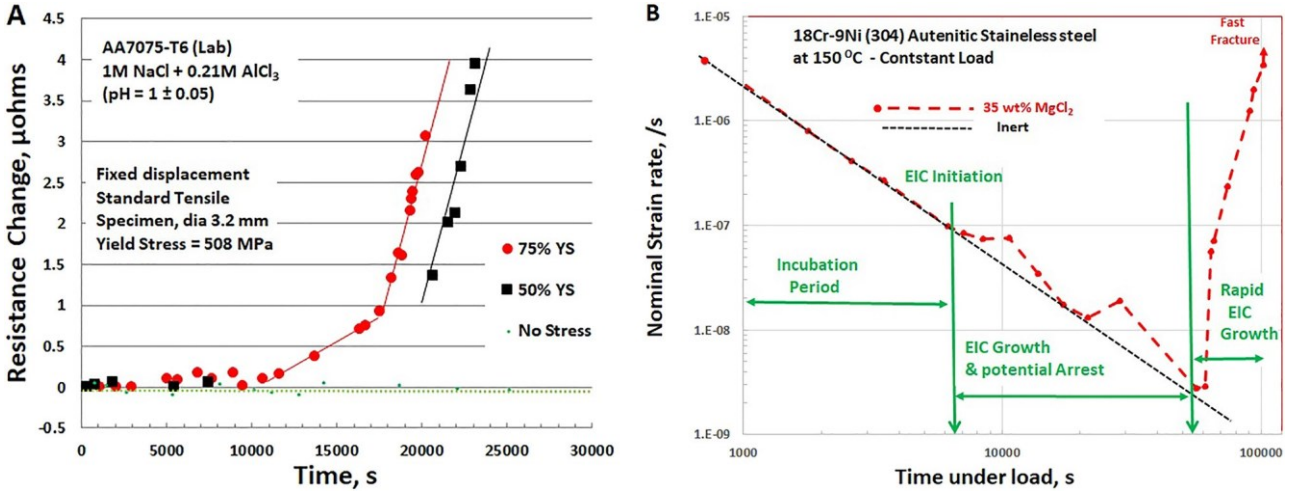

Figure 2: Experimental data showing the proposed 3 steps for EIC (precursor, initiation/early growth and crack propagation): (A) electrical resistance change during EIC testing AA7075-T651 tensile samples (0.75 % YS) fully immersed in 1M NaCl + 0.21M $AlCl_3$ (pH = 1) while potentiostatically held at −1100 mV (SCE) at room temperature, McHardy and Hllingsworth (1966) and (B) nominal strain rate estimated from extension-time behavior generated during constant load testing annealed18Cr–8Ni (304) stainless steel immersed in 35 % $MgCl_2$ at 150 °C reported by Bleckmann and Zitter (1974).

on an amalgamation and extension of proposals by others (Jones and Simonen 1994; Parkins 1988; Persaud et al. 2019; Staehle 2008, 2010).

2.1 Specific adsorption of chemical species

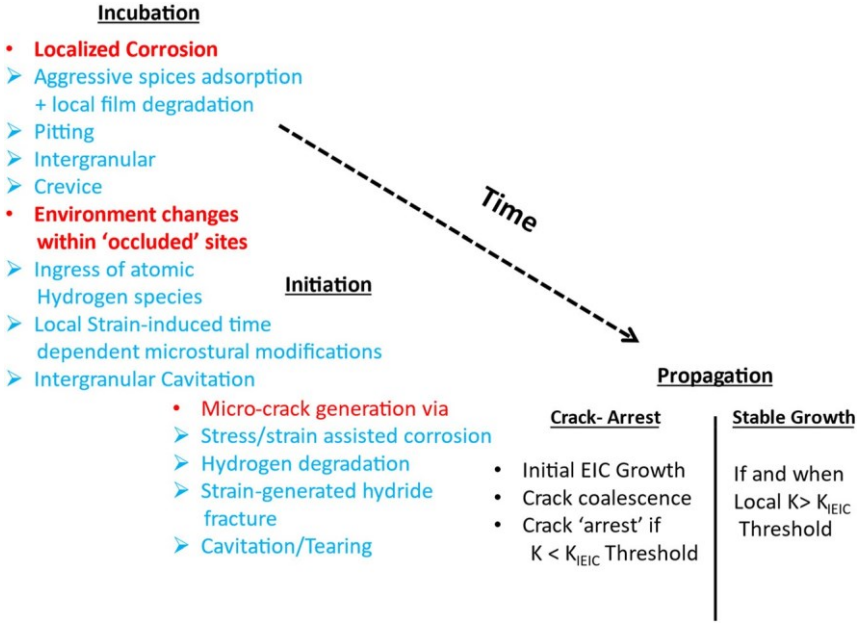

Figure 3: A schematic showing potential phenomena during the three phases of EIC.

The role of the specific adsorption of chemical species during the precursor period and any subsequent EIC microcrack initiation remains controversial, and was the subject of extensive written discussions between Uhlig and Bockris, Kruger and Pourbaix, Uhlig (1977) and Parkins and Kruger, Pugh and Uhlig, Parkins (1977) following papers presented at a key International Conference in 1973 (NACE-5) in France.

During the late 1930s and following WW2, a group of researches in the USSR (Rehbinder 1947) conducted a series of physico-chemical evaluations of the deformation of various solids (rocks and metals) while surrounded by 'surface-active' species and proposed a 'New physico-chemical phenomena in the deformation and mechanical treatment of solids' (Rehbinder 1947). The phenomena, subsequently known as the 'Rehbinder Effect', was proposed to involve the penetration (adsorption) of 'surface-active' species into ultra-microscopic cracks formed during the

strain-hardening of the immediate surface layers during early deformation, that reduced a metals resistance and locally enabled crack extension (Barlow 1966). Another explanation, Andrade and Randell (1949) proposed the adsorption of 'surface-active' species promoted a 'disintegrating action' to the surface oxide film that otherwise would have provided strength.

Subsequent suggestions for the role of specific adsorption a decade or so later, proposed: that a) EIC initiation and propagation in aqueous environments is brittle fracture, where the surface energy associated with crack formation is reduced by the adsorption of specific ions (Coleman et al. 1961) and b) Selective adsorption of specific ions after lowering the surface energy of cracks can operate conjointly with electrochemical action (Uhlig 1959) at potentials above a critical value (Uhlig and Cook 1969) along paths, where defects predominate and where compositional gradients exist.

In more recent times, compelling evidence, based on high-resolution electron microscopy fractography, presented inaseriesofreview articles byLynch (1977, 1988, 2013)suggest specific adsorption can play a role during EIC propagation for a range of metallic materials including aluminum alloys, nickel, iron-silicon, high-strength steels, magnesium, and titanium alloys when exposed to various aqueous environments. Additionally, similarities were proposed between hydrogen-assisted cracking, stress corrosion cracking, and adsorption-induced liquid-metal embrittlement.

Interest in the role of specific adsorption has continued with further experimental and modelling work to elucidate the role played by mechanochemical and chemomechanical surface effects during the EIC and fracture of metal alloys (Bogdanov et al. 2019; Gutman et al. 1996; Yan et al. 2023; Yin and Yuan 2023).

2.2 Incubation (precursor) process step

Historically the incubation (precursor) step ahead of EIC microcrack initiation has received minimal attention and is the least well understood process step. There has been limited activity for aluminum and magnesium alloys (Cocks et al. 1959; Logan 1961) and copper-based alloys (Pugh 1971) at ambient temperatures, slightly more for carbon steels (Parkins 1988) and somewhat more, for stainless steel and nickel-based alloys at elevated temperatures as used in the fossil and nuclear power generation industries (Arioka et al. 2010, Arioka 2020; Gooch 1984; Lees and Siverns 1978).

Depending on the metallic alloy-environment system involved the incubation (precursor) step can be completed within a few seconds, as shown by sudden failure of stressed hard-drawn 13-carat gold thick-wire exposed to a small volume of ferric chloride, Roberts-Austen (1888), to longer times, from a few hundred to a few thousand hours for austenitic stainless steels in concentrated magnesium chloride solutions at around 150 °C (Bleckmann and Zitter 1974; Desjardins et al. 1980). This step can last for up to a decade or more for carbon steels exposed to deoxygenated steam at 360 °C in fossil-fueled power plants (Lees and Siverns 1978) to even longer times, up to 40 years, for hydrogenated reactor coolant at 310 °C in a pressurized heavy water reactor (PHWR) observed in light-water nuclear reactors (Arioka et al. 2013).

These observations confirm that the critical events during the incubation (precursor) stage differ between metallic alloy-environment systems especially when complications introduced by an alloys initial surface condition and its immediate sub-surface layers with 'disturbed microstructures' (Beilby 1921; Chang et al. 2019; Forsyth 1998; Paxton and Procter 1968; Scamans et al. 2010) generated during manufacture or fabrication for industrial use or during laboratory test specimen preparation.

However, despite of these limitations, we have identified two basic EIC precursor categories:

- Micro-crack initiation following incubation directly from or within a few microns of an external 'smooth' surface exposed to bulk environments and
- Micro-crack initiation from within an occluded geometric feature generated during the precursor process and now containing modified local environmental conditions (solution chemistry and electrochemical potential) from the bulk environment.

We have considered the end-point of these two categories to be equivalent, with the caveat being that the development of an appropriate local environmental and stress raiser conditions needed for EIC micro-crack initiation under full immersion, alternate immersion or thin-electrolyte-layer conditions (e.g. under humid air environments).

Edeleanu and Evans (1951) prediction that local environmental changes should occur within occluded regions was experimentally verified by the measurement of local solution pH changes within unstressed restricted geometries for nonferrous and ferrous alloys exposed to a saline solutions (Alavi and Cottis1987; Brown et al. 1969; Cooper and Kelly 2007,2008; Davis1971a,b;Holroydetal. 1984,1987;Kelly2021;Sandozet al. 1970). Additionally,

extensive modelling has been conducted on the development of electrochemical potential and local solution chemistries with restricted geometries for aluminum alloys under full immersion conditions in aqueous saline environments without the application of load (Edwards 1990; Cooper and Kelly 2007, 2008; Kelly 2021).

For ferrousalloys, Turnbullandcoworkers(Turnbull1993, 2001, 2017, 2021; Turnbull et al. 2009) modelled the complex processes involved during the EIC initiation process that included: electrochemical potential and solution chemistry development within restricted geometries (Turnbull 1990, 2001), the 'pit-crack' transition (Turnbull 2017, 2021; Turnbull and Zhou 2004; Turnbull et al. 2009) and a strain-based rationalization (Horner et al. 2011; Turnbull 2017) as to why EIC initiation can occur towards the open end of pits or occluded regions, rather than at the deepest penetration where the local mechanical stress would be higher. A recent review of the governing factors for pit-to-crack transitions of metallic structures came to similar conclusions (Katona et al. 2023). However,verylimitedinformationisavailablefor anymetallic alloys under load or for alloys under alternate immersion or thin-electrolyte-layer conditions with or without load.

2.2.1 Influence of deformed surface layers

Deformed surface layers generated during metal processing can control EIC initiation during both in laboratory testing and in commercial applications.

Contrastingresponseshavebeenreportedforanaustenitic stainless steel strained in boiling magnesium chloride at 144 ˚C (Kohl 1967) and commercial carbon-manganese pipeline steels strained in 0.5 M Na_2CO_3 + 1M $NaHCO_3$ solution at 70 ˚C (Wang and Atrens 1996), compared to an Al–Zn–Mg alloy strained in a saline environment at 25 ˚C (Borchers and Tenckhoff 1969). Significantly longer EIC initiation times resulted after the removal of deformed surface layers generated by machining for both the 18Cr–9Ni austenitic stainless steel, with an electropolished surface following (Table 3) and for carbonmanganese pipeline steels with a lightly machined (Table 4).

Significantly longer EIC initiation times resulted when deformed surface layers were removal from an Al–Zn–Mg alloy subjected to constant load testing in a saline environment at 25 °C, Borchers and Tenckhoff (1969), Figure 4.

Table ?: Effect of deformed surface layer removal on the EIC initiation times for ??Cr–?Ni austenitic stainless steel subjected to constant load testing at ??? MPa (?? % UTS) in boiling ?? % $MgCl_?$ solution at ???°C, Kohl (????).

Surface condition	Time (s)		
	EIC initiation	Crack propagation	Final fracture
Machined + final light electropolish (? tests)	???	?,???	?,???
Oversized machined + final ??? µm electrochemical surface removal (?? tests)	?,???	?,???	?,???

Table ?: Effect of surface condition on minimum stress for EIC initiation in X?? pipeline steel (yield stress ??? MPa) in ?.? M $Na_?CO_?$+?M $NaHCO_?$ solution at ??°C under potentiostatic control under increasing load.

Potential (mV, SCE)	EIC minimum stress (MPa)	
	Original surface	Polished surface
–???	???	???
–?,???	???	???

Data from Wang and Atrens (????).

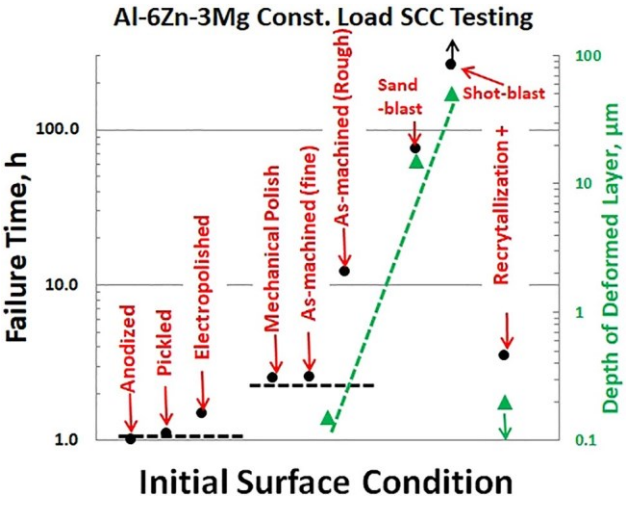

Figure 4: Failure times for an underaged Al–6Zn–3Mg alloy for a range of surface pretreatments prior to constant-load testing at 147 MPa in 0.53M NaCl + 0.1 % H_2O_2 environment held at 25 °C. Data taken from Borchers and Tenckhoff (1969).

Deformed surface layers on the 18Cr–8Ni stainless steel and carbon-manganese pipeline steels are prone to suffer local fracture at relatively low stresses and provide local EIC initiation sites and hence their removal is beneficial, whereas for the Al–Zn–Mg alloy disturbed layers typically are not brittle and their presence prevents or delays environmental access to the underlying alloy bulk microstructure (i.e.

removal is detrimental). For aluminum alloys, the deformed layer has a different microstructure with an ultrafine grain size to the bulk material (Beilby 1921; Forsyth 1998; Paxton and Procter 1968; Scamans et al. 2010), that can control EIC initiation behavior, or simply delay the environment having direct access to the underlying bulk alloy.

2.3 Micro-crack initiation and early growth

The transition between incubation (pre-cursor) and microcrack initiation and early crack growth remains a poorly understood aspect of EIC initiation. The local mechanics of micro-crack initiation can be considered as insensitive to whether it occurs, near to an external free-surface, involving the bulk environment (Figure 5A) or from within an occluded region (say from 50 µm up to a few mm deep) that usually contains a locally modified environment different from the bulk, Figure 5B.

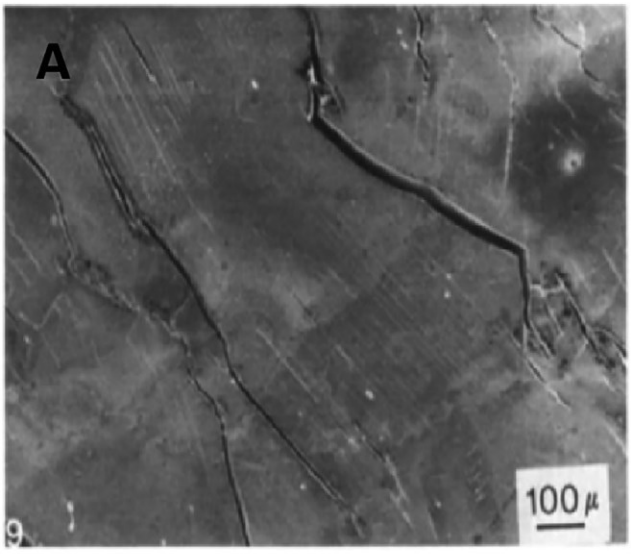

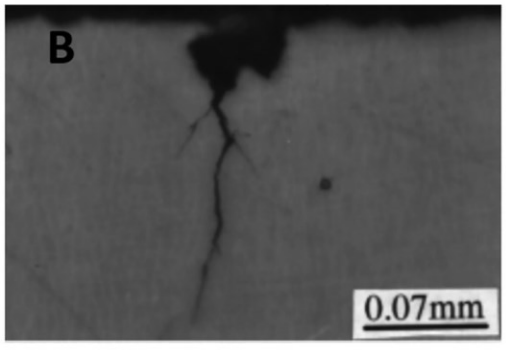

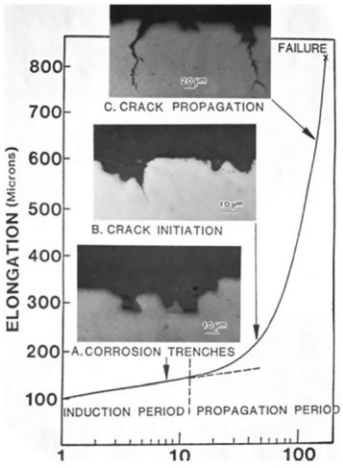

Figure 5: Intergranular EIC initiation: (A) associated with Transgranular surface slipsteps generated during the slow strain rate testing 70/30 α-brass in 1M $NaNO_2$ at RT, while held potentiostatically at −100 mV (SCE) [Image taken from Yu et al. (1984)], and (B) from within localized corrosion sites generated during the early stages of constant load testing a 26Cr–1Mo ferritic stainless steel at 90 YS, while potentiostatically held at −460 mV (SCE) and immersed in boiling 42 % LiCl + 1 % thiourea. Localized corrosion site geometry development as a function of test time in minutes. [Images take from Kwon et al. (1992) and Locci et al. (1987) used with permission from ©AMMP 2024].

Initial EIC crack growth is typically restricted to approximately one grain diameter with cracks terminating on reaching a microstructural barrier. In instances where deeper cracks evolve, sometimes by interacting and coalescence with other cracks (Connolly and Scully 2000; Elboujdaini et al. 2000; Parkins and Singh 1990), growth of these micro-cracks are highly sensitive to and controlled by local EIC susceptibility and microstructure, together with whether a sufficient local mechanical driving force is available to fracture any uncracked ligaments in the cracked regions process zone that otherwise would result in crack arrest.

Processes controlling initial EIC micro-crack growth typically involves either anodic dissolution or a hydrogeninduced process, which for some alloy/environment systems may be controlled potentostatically or by pre-exposure or cathodic pre-charging with hydrogen.

2.3.1 Crack arrest during the initiation process

EIC has been reported to initiate under static loading conditions well below those necessary to enable sustained EIC propagation in magnesium alloys (Wearmouth et al. 1973), carbon-manganese steels (Parkins and Greenwell 1977), aluminum alloys (Holroyd et al. 2015; Liu et al. 2004, 2007; Schra and Wanhill 1997, 1999) and HSLA steel and conventionally quenched and tempered low alloy steel (Kumar 2008) exposed to aqueous saline solutions at ambient temperatures.

A schematic illustration of this behavior under constantload conditions is shown in Figure 6.

Experimental evidence of this behavior is shown in Figure 7, using data for a 0.05 % carbon steel under constant load testing and potentiostatic control in an aqueous carbonate/bicarbonate solution at 90 ˚C (Parkins and Greenwell 1977). EIC cracks can initiate and arrest when the applied stress is below a minimum, $\sigma_{Thresshold}$, Figure 7A. The maximum implied stress intensity factor for the measured 'arrested' cracks (calculated here assuming penny-shaped elliptical cracks) is similar to the experimentally measured threshold stress intensity for EIC, K_{IEIC}, Figure 7B.

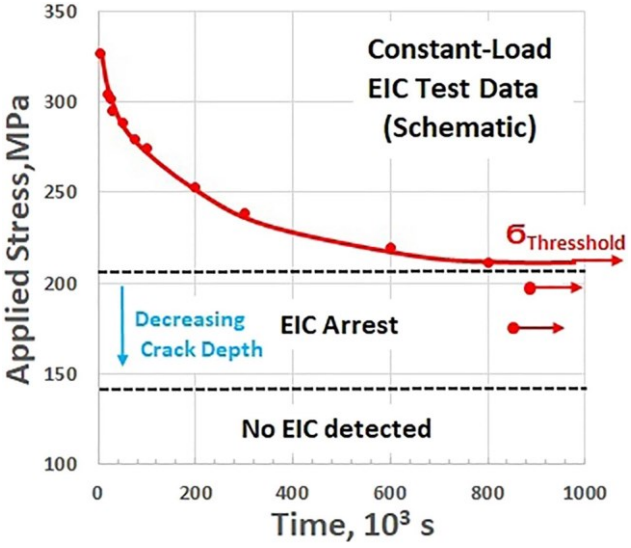

Figure 6: A schematic representation of hypothetical constant-load EIC test behavior showing that EIC can initiate at applied stress levels below the threshold needed to ensure propagation to failure, $\sigma_{Thresshold}$, but subsequently arrest.

Another schematic representation of 'EIC arrest' is provided in Figure 8. Here EIC initiation and its subsequent arrest is superimposed upon crack growth rate – stress intensity factor data from classic double cantilever beam EIC testing of a fatigue pre-cracked test specimen loaded under constant-defection conditions, where the applied stress intensity factor decreases with EIC growth and provides a EIC threshold stress intensity factor, $K_{IEIC(Macro)}$ for a long crack, based on when crack growth rates fall below about 10^{-11} m/s.

Schra and Wanhill (1997, 1999) reported experimental data that confirmed the initiation and arrest of EIC at K levels well below the reported threshold, K_{IEIC} for a high-strength aluminum alloy undergoing EIC in a saline solution, which was analyzed by Holroyd et al. (2023).

The local conditions needed for EIC initiation and whether EIC arrests or continues to propagate are highly sensitive to prevailing local microstructural strainaccommodation characteristics, which is both time and temperature-dependent.

EIC evaluation or the approval/verification testing of metallic alloys rarely assess crack initiation, other than via the assumed relationship with a threshold stress, σ_{EIC} or stress intensity factor, K_{IEIC}, obtained for arresting 'long cracks' in pre-cracked test specimens. While a higher K_{IEIC} is indicative of an improved EIC resistance to crack propagation, an arrested 'long crack' in a pre-cracked test specimen may not be representative or relatable to EIC initiation where this is no pre-existing crack.

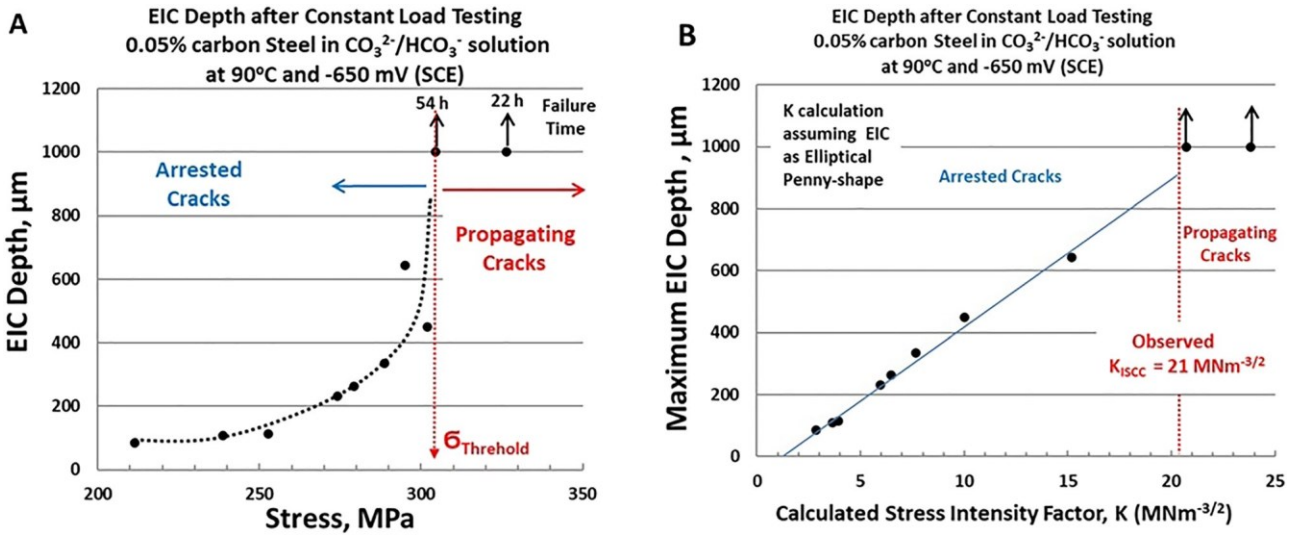

Figure 7: Depth of arrested intergranular EIC in tensile samples developed during constant-load testing of a 0.05 % carbon steel in a carbonate/bicarbonate environment at 90 ˚C under potentiostatic control at −650 mV (SCE): (A) EIC depth as a function of applied stress and (B) estimated stress intensity factors for arrested EIC, assuming a half-penny-shaped crack profile. Applied stress and maximum crack depth data taken from Parkins and Greenwell (1977) and estimated stress intensity factors calculated by current authors.

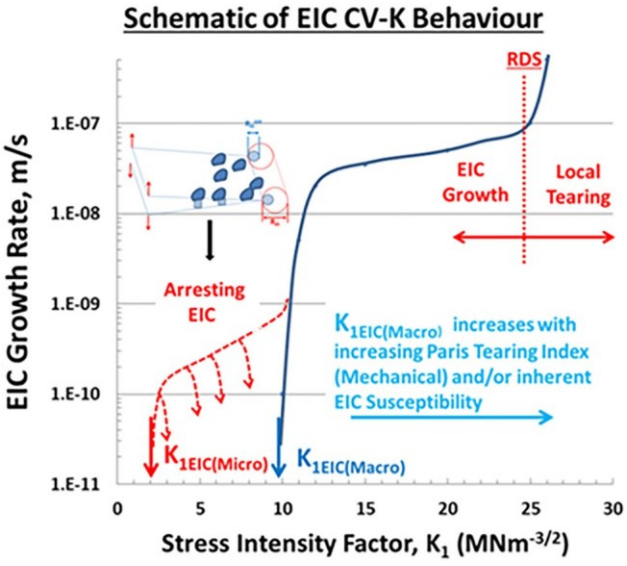

Figure8: Schematic representation of EIC with micro-crack initiating and arresting at K's below K_{IEIC}, using data for a high-strength aluminum alloy, but applicable to other metallic alloys. Taken from Holroyd et al. (2023); reproduced with permission from © AMMP 2023.

2.4 Role of local microstructural strainaccommodation characteristics

Although it had been considered that strain-accommodation by creep-like processes are unlikely to be relevant for temperatures below 0.4 T_M, experimental evidence for several ferrous and non-ferrous metal/environment systems shows that the exhaustion of primary creep in an inert environment ahead of exposure of a stressed alloys to an EIC environment can either prevent EIC initiation or can significantly increase the minimum mechanical driving force ($\sigma_{Thresshold}$ or K_{IEIC}) required for EIC initiation at ambient and elevated temperatures, Table 5.

Leckie (1967) showed significant differences in EIC initiation behavior for fatigue pre-cracked cantilever beam tests specimens of annealed titanium alloy (Ti–7Al-2Cb-1Ta) loaded in laboratory air (30 % RH) and then exposed to 0.53M NaCl with and without a time delay of a few minutes to enable beam deflection rates to become stable after loading as shown by Kujawski and Krempl (1981). The introduction of a time delay after loading enabled sufficient primary creep exhaustion to prevent EIC initiation at stress levels that would have promoted EIC initiation, Figure 9. These finding suggest that EIC initiation requires a sufficient local strain rate in addition to a mechanical load. Leckie (1967) attributed the local minimum strain rate requirement to that needed to disrupt a thin protective oxide film.

Similar findings by Kwon et al. (1992) have been reported for EIC initiation in a mill-annealed low-interstitial 26Cr–1Mo ferritic steel (E-Brite) subjected to constant load testing in a boiling 42 % LiCl solution, while polarized to potentials above the critical cracking potential, E_{cc}, Uhlig

Table 2: Examples of ferrous and non-ferrous metal/environment systems where exhaustion of primary creep ahead of exposure of a stressed sample to the EIC environment can either prevent or significantly increase the minimum mechanical driving force ($\sigma_{Thresshold}$ or K_{IEIC}) required for EIC initiation.

Alloy	Loading conditions	Environment conditions	Temperature	T_m (T/T_{mp}) °K	References
Ti–2Al-2Cb-2Ta Annealed YS = 222 MPa, UTS = 333 MPa, K_{IC} = 222 $MNm^{-3/2}$	Fatigue pre-cracked SEN cantilever bend, constant load	Lab air (22 % RH) or 2.22M NaCl, FCP	RT	0.22	Leckie 2222 (Figure 2)
Mg–2Al	Constant load, smooth tensile specimen		RT	0.22	Wearmouth et al. (2222)
22Cr–2Mo ferritic stainless steel	Constant load, smooth tensile specimen	22 % LiCl + thiourea, –222 or –222 mV (SCE), de-aerated	222°C	0.22	Kwon et al. 2222 (Figure 22)
Annealed 222 stainless steel K_{IC} = 22 $MNm^{-3/2}$	Constant strain, notched WOL, constant load, SEN both with 0.2 mm notch root radius	22 % $MgCl_2$	222°C	0.22	Gu et al. 2222 (Figure 22)
As-quenched NiCrMoV rotor steel, YS = 2,222 MPa	Double cantilever beam, fatigue pre-cracked, constant load & constant strain	Dry air, (silica–gel), distilled water	22°C	0.22	Rieck et al. 2222 (Figure 22)
As-quenched 2,222 high strength martensitic steel, YS 2222 MPa	Double cantilever beam, fatigue pre-cracked, constant load & constant strain	Dry air, (silica–gel or P_2O_5), distilled water	22°C	0.22	Rieck et al. 2222 (Figure 22)
C–Mn pipeline steel	Constant load fatigue pre-cracked SEN cantilever bend	2M Na_2CO_3 + 2M $NaHCO_3$, –222 or –222 mV (SCE)	22°C	0.2	Parkins 2222 (Figure 22)

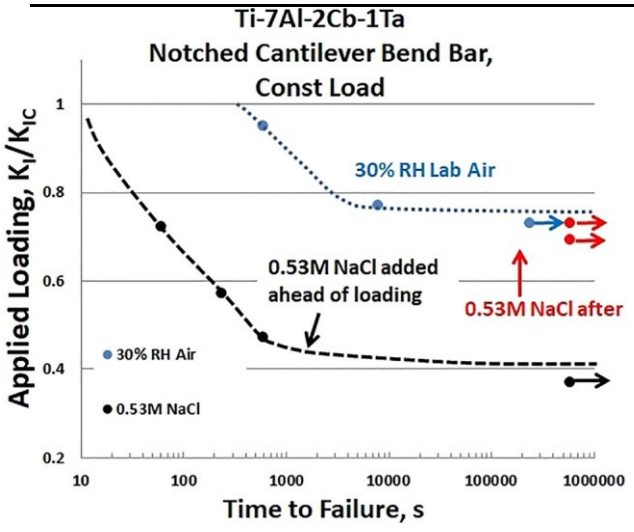

Figure 9: Failure time for annealed titanium alloy (Ti–7Al-2Cb-1Ta) fatigue pre-cracked cantilever beam test specimens loaded in laboratory air (30 % RH) and then exposed to 0.53M NaCl or 30 % RH laboratory air. Data from Leckie (1967).

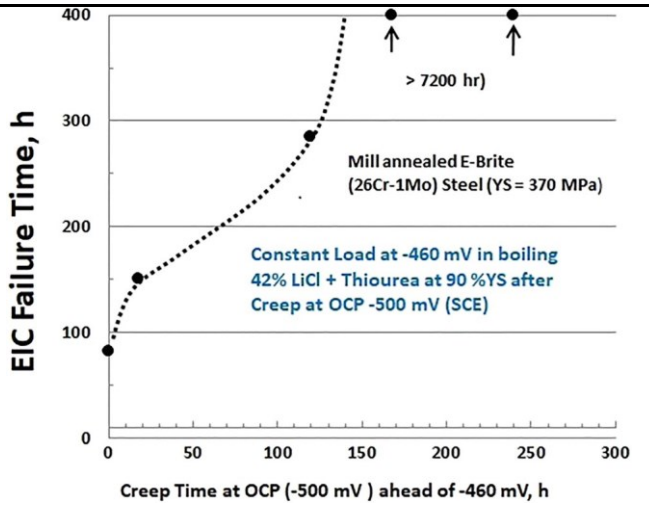

Figure 10: EIC failure time for mill annealed E-Brite ferritic stainless steel subjected to constant-load testing in 42 % LiCl + thiourea polarized at –460 mV (SCE) as a function of initial holding time under load at a 'noncracking' potential (–500 mV (SCE)) to allow primary creep exhaustion. Data taken from Kwon et al. (1992).

(1959). EIC initiation was prevented by allowing primary creep exhaustion at the corrosion potential ahead of increasing the potential to above E_{cc}, where otherwise EIC would have initiated, Figure 10.

Although similar findings were reported for an annealed 304 stainless steel exposed to boiling 42 % $MgCl_2$ under fixed-displacement conditions, Gu et al. (1994), Figure 11, when testing was repeated under a constant load the allowance of 72 h creep under the test load conditions at

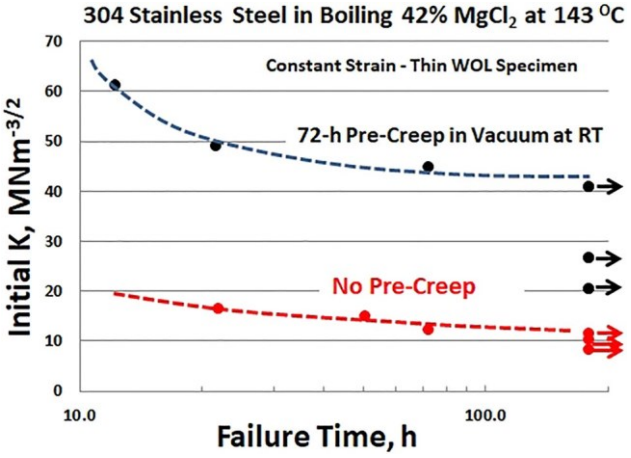

Figure 11: Failure time for annealed 304 stainless steel single-edge 0.2 mm notch root diameter test specimens exposed to 42 % boiling $MgCl_2$. Data extracted from Gu et al. (1994).

Table ?: K_{ISCC} data quoted by Gu et al. (????) from annealed ??? stainless steel notched test specimens subjected to constant strain or constant load EIC testing in a boiling ?? % $MgCl_?$ solution, with and without ?? h precreep under load prior to the addition of the test environment.

EIC threshold stress intensity factor, K_{ISCC} ($MNm^{-?/?}$)		
Loading mode	No pre-creep	Pre-creep
Constant strain	??.?	??.?
Constant load	?.?	?.?

either room temperature or 142 °C ahead of adding the aqueous environment had no significant effect on the failure time or the implied EIC threshold stress intensity factor, K_{ISCC}, Table 6.

For austenitized and oil-quenched NiCrMoV Rotor Steel and high-strength 4,340 steel, Rieck et al. (1989) demonstrated EIC initiation was prevented in fatigue pre-cracked double cantilever beam (DCB) test specimens loaded to 40 $MNm^{-3/2}$, following 10 min creep exhaustion under fixed-displacement conditions in an inert environment (P_2O_5 dried air) after 1 h drying (unloaded) ahead of loading with exposure to distilled water at 22 °C. EIC initiation is prevented, despite the applied K being well above the published K_{IEIC} threshold of 10– 20 $MNm^{-3/2}$ (Magdowski 1987). Similar testing using silica gel dried air was sufficient to prevent EIC initiation for the Rotor Steel but not for the 4,340 steel, Figure 12.

Parkins (1979) demonstrated the importance of local strain rate deformation rates during EIC initiation as shown in Figure 13 for constant load testing of fatigue pre-cracked notched cantilever beam specimens of a carbon-manganese steel exposed to a 0.5M Na_2CO_3 + 1M $NaHCO_3$ solution at 75 °C, under potentiostatic control.

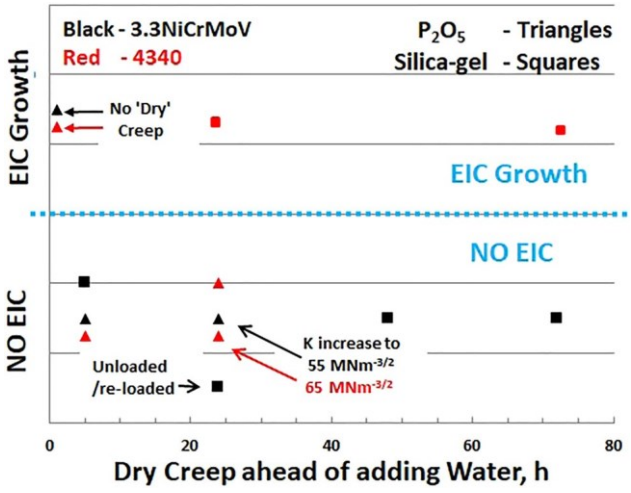

Figure 12: Use of creep exhaustion in an inert environment to prevent EIC initiation in as-quenched high strength steel (4,340) and 3.3NiCrMoV Rotor steel pre-cracked DCB test specimens load to initial K of 40 $MNm^{-3/2}$. Data extracted from Rieck et al. (1989).

The unique aspect of these results using two electrochemical potentials during straining is the confirmation that EIC initiation and growth in the system studied requires both an appropriate electrochemical potential, −650 mV (SCE) and an adequate local crack-tip region strain rate.

2.5 Crack arrest and crack coalescence during the initiation process

Characteristic extension-time creep behavior for metal wire or waisted tensile sample subjected to a constant load in an inert environment is shown in Figure 14. The data shown for an austenitic stainless steel strained in an inert oil at 154 °C provided by Desjardins et al. (1980) initially displays characteristic rapid extension (primary creep) followed by a

transition to an exponentially decreasing extension rate (secondary creep) Figure 14A, with the overall extension behavior following logarithmic time dependence, Figure 14B.

Nominal strain rates promoted during constant load testing may be estimated as a function of time by using the slope of the extension-time curve, nomalized using the test specimen gauge length. Such estimated are shown in Figure 2B for 304 austenitic stainless steel tensile samples subjected to constant-load testing in oil or 35 % $MgCl_2$ at 150 ° C by Bleckmann and Zetter (1974). Implied nominal strain rate response in inert environments decease linearly logarithmically with time, whereas any increases in nominal strain rate during testing in the $MgCl_2$ reflects EIC initiation, and any subsequent decrease are associated with local micro-crack arrest, Figures 2B and 15.

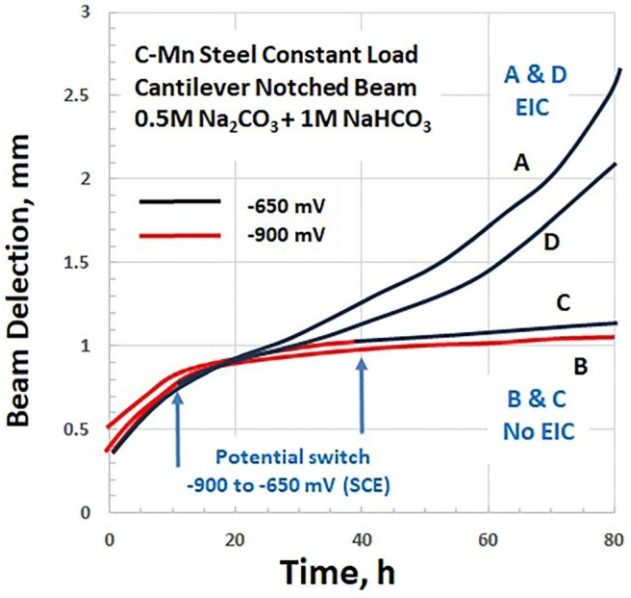

Figure 13: Cantilever beam defections under constant load provided by Parkins (1979) for a C–Mn pipeline steel immersed in a carbonate/ bicarbonate solution at 75 °C as a function of time at the potentials for four test conditions: Curve A: at −650 mV (SCE) throughout the test, shows increasing deflection at a rate increasing with time, especially after the initial stages of testing. EIC initiation and growth, confirmed post-test. Curve B: at −900 mV (SCE) throughout the test, shows a continual decrease in the deflection rate consistent with creep exhaustion and lack of EIC initiation detected post-test. Curve C: at −900 mV (SCE) for the initial 40 h, while the observed deflection rate decreased to a relative steady rate indicative of primary creep exhaustion, and then switched to −650 mV (SCE), which resulted in no significant change to deflection rate behaviour, consistent with the lack of any EIC initiation found after testing. Curve D: at −900 mV (SCE) for the initial 12 h of loading, while the observed deflection rate did not decrease significantly switching to −650 mV (SCE) led to an increasing deflection rate, similar to that found for testing at −650 mV (SCE). EIC initiation and growth was confirmed post-test.

Analysis of the Bleckmann and Zitter (1974) constantload data shows that the implied EIC initiation and subsequent arrest behavior for 304 austenitic stainless steel immersed in a less aggressive environment, 20 % $MgCl_2$ at 150 °C, Figure 15, is indicative EIC initiation now requires a longer incubation period and additional time for the crack growth needed for onset of rapid EIC as opposed to crack arrest.

2.6 Opportunities/needs for additional research/investigation of EIC in additively manufactured materials

Recent reviews have highlighted the need for EIC research (Lewandowski and Seifi 2016) on selected corrosion-resistant materials (Biserova-Tahchieva et al. 2023) processed via AM

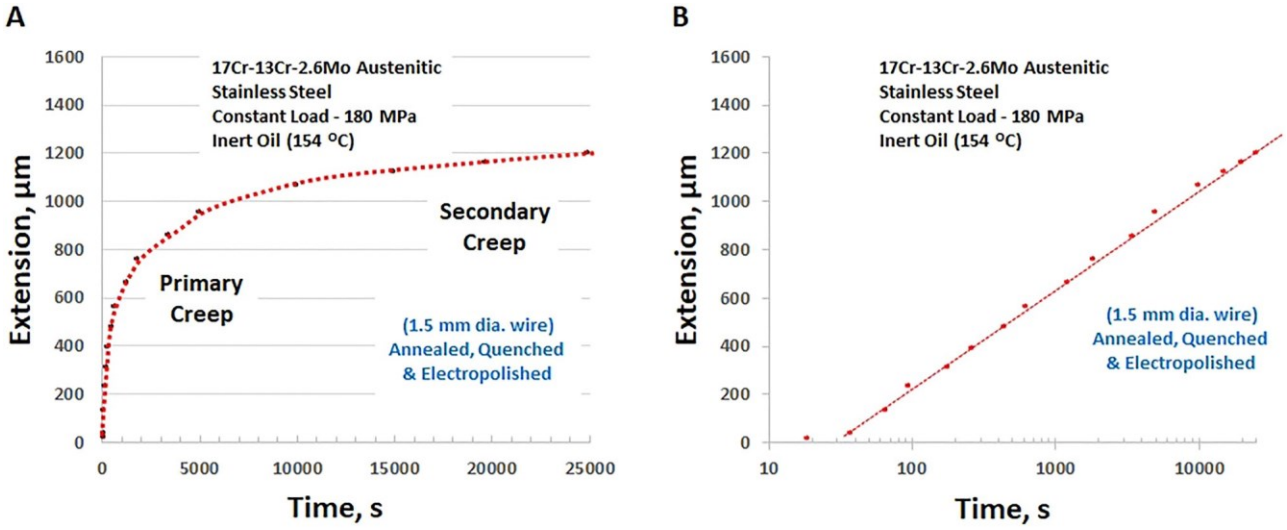

Figure 14: Characteristic extension-time response for a metal alloy under a constant-load in an inert environment. Data taken from Desjardins et al. (1980) for an annealed austenitic steel loaded exposed to an inert oil at 154 °C: (A) extension as a linear function of time, showing an initial high extension rate associated with primary creep followed by an exponentially decreasing rate associated with secondary creep, (B) extension data from (A) replotted as a logarithmic function of time.

techniques. As pointed out by Lewandowsi and Seifi (2016) AM processing has mainly focused on conventional alloys that were not necessarily designed to be processed via AM techniques. This is an important consideration as AM processing may produce a variety of non-equilibrium microstructures (e.g. due to the rapid solidification), nonequilibrium segregation of alloying elements, as well as process-induced defects such as keyholes, lack of fusion, solidification porosity, and as-processed surface roughness. These aspects may completely change the EIC response of as-processed as well as post-processed materials using conventional post-processing techniques (e.g. heat treatment, HIP, etc.) as the heat treatment response of such AM-processed materials may be completely different than that exhibited in conventionally processed materials (e.g. cast, rolled, forged, etc.). While EIC studies on AM processed materials are emerging (Rebak and Lou 2018; Santamaria et al. 2023; Yazdanpanah et al. 2022), which suggest the EIC propensities of AM materials will be at least equivalent to conventional alloys, a need exists to extend additional effort to identify novel surface/bulk post-processing techniques to specifically target EIC prevention for both AM and conventional metallic products.

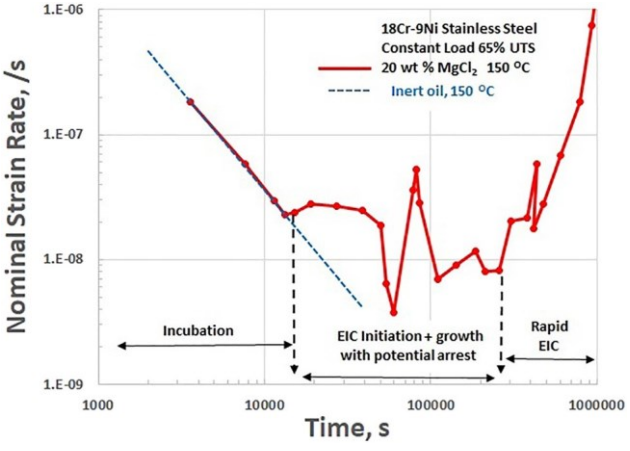

Figure 15: Nominal strain rate obtained from extension-time behavior generated during constant load testing annealed 18Cr–8Ni (304) stainless steel immersed in 20 % $MgCl_2$ at 150 °C. Data obtained from Bleckmann and Zitter (1974).

2.7 Opportunities based on new characterization capabilities

There is an opportunity further insight into the understanding of EIC initiation based on some of the latest characterization capabilities. However, this it is still a significant challenge as the time scale of initiation could be almost instantaneous in terms of the moment an EIC crack appears from something that was a crack precursor and this may happen following a significant time which practically could be days, weeks or years and in laboratory experiments could still be many hours. This could be a major issue restricting the use of highly time-resolved probes to investigate initiation involving huge data streams and 'wasted' equipment time to move past incubation

and capturing initiation events. Similarly, the location of initiation events can be widely distributed across a sample surface, and it is not possible to know exactly where the initiation event will occur. It is a challenge to maintain high spatial resolution analysis over a large area. Reducing the area observed or creating pre-cursor features such as pre-cracks, will localize initiation but this may not represent the real situation depending on the application where initiation occurs on preferred sites and not pre-cracks.

The direct detection of hydrogen using mass spectrometry techniques of NanoSIMs (Li et al. 2020) and atom probe tomography (APT) (Gault et al. 2012), Hydrogen trapping and embrittlement in high-strength Al alloys (Zhao et al. 2022) can be used to support predictions of hydrogen trapping at specific microstructural locations. NanoSIMS is capable of mapping a surface with a resolution between 50 and 200 nm to detect hydrogen and APT is capable of near atomic resolution. However, the sample preparation and ultra-high vacuum characterization environment make it very difficult to preserve the distribution of hydrogen in the microstructure and this may be limited to identification only of deep traps where the hydrogen atoms are relatively stable. Cryopreparation, transfer and measurement are helping to address this issue (McCarroll et al. 2000). Another opportunity is based on the use of deuterium or other isotopic labels to identify exactly which source of environment is responsible for the observed features e.g. fracture path and can separate this hydrogen source from any background or any hydrogen pre-existing in the metal. An investigation of the oxidation behavior of zirconium alloys using isotopic tracers and high-resolution SIMS (Yardley et al. 2013) and NanoSIMS analysis of hydrogen and deuterium in metallic alloys: Artefacts and best practice (Aboura and Moore 2021).

Neutron imaging and diffraction is another technique which can directly detect the presence of hydrogen (Griesche et al. 2014). Three-dimensional hydrogen distribution and quantitative determination of titanium alloys via neutron tomography (Yang et al. 2020). However, acquisition times are long and resolution is relatively low in the 10′ s of microns range. But it is non-destructive and non-contact which meansin situ studies which preserve the test environment can be conducted. The resolution is a limiting factor as it does not match the scale of the microstructural features where hydrogen is trapped.

Scanning Kelvin probe microscopy, following a specific methodology of sample preparation can also be used to detect and spatially map hydrogen (Ma et al. 2021) This time at a scale of 10 s of nanometres and typically across a 100 μm or less field of view. It is well suited to studies of initiation especially from corrosion sites based on it′s very high spatial resolution, and capability to work in liquids and to conduct time-lapse studies (Blanc and Oltra 2023). It is however limited to surface analysis.

Whilst X-ray computed tomography cannot directly detect hydrogen it is a high-speed, high resolution technique which with synchrotron sources is capable of observing fast fracture in 3D over time (Maire and Withers 2014). This technique can provide the requisite microstructural scale and as a non-destructive, non-contact technique tests can be conducted in any environment and directly observed. This means that it is now possible to see the influence of different environments or strain conditions on the failure/fracture process (Gudla et al. 2020; Koko et al. 2023; Singh et al. 2014). Combination of X-ray diffraction and X-ray scattering and spectroscopy techniques are also gaining attention to add additional structural and chemical information (Kim et al. 2023) although itcan bechallenging tooptimize the conditions for materials testing, imaging and diffraction simultaneously especially for time-resolved experiments (King et al. 2008; Örnek et al. 2023). The technique is extremely powerful for understanding different behaviour as cracking evolves and relating it directly to post-mortem studies which might typically involve electron microscopy fractography but can also includeother techniques such asnanoSIMS and APT.The nondestructive, non-contact nature of neutron and X-ray tomography also means that many different probes can be used during testing to observe, mechanical, electrical, chemical and other changes taking place during experiments.

Relatively simple experimental setups using optical microscopy (Euesden et al. 2023) or highly sensitive detection using electrical probes for mechanical (Crane and Gangloff 2016; Harris et al. 2016) or electrochemical detection (Yang et al. 2016) can also be extremely effective and have the advantage of being simple and allowing many repeat tests to be carried out.

In all of the above techniques it is often difficult to properly capture the critical microstructural scales which covers at the upper end, many grains and the second phase particles as well as the nanoscale particles and atomic scale interfaces which are of critical in determining EIC susceptibility. Especially as to appreciate the creep or time-dependent strain behaviour of a metal requires detailed examination across multiple grains and the capture of evolving microstructural information. X-ray diffraction can achieve this in a nonspatially resolved way but latest in situ scanning electron microscopy techniques (Taylor et al. 2024; Yavuzyegit et al. 2023)are enabling microstructurally resolved studies covering a wide range of scale whilst extracting

quantitative structural details (Gutierrez-Urrutia et al. 2013; Wang et al. 2023). However, challenges still remain to apply to capture the influence of the environment.

Although these techniques are extremely powerful, they are not able, individually to give all the perspectives needed to understand EIC and the incubation and initiation of cracks (Koyama et al. 2017). The temporal and spatial scales that have to be traversed as well as the environmental, mechanical and microstructural context means that our best chance of studying EIC initiation is through a multimodal, multiscale and correlative approach (Burnett and Withers 2019).

3 Conclusions

Experimental evidence for EIC for a wide range of metallic alloy systems, including: aluminum, magnesium, titanium, high and low strength and stainless steels and nickel alloys has shown that:

EIC Initiation and propagation involve two timeresolved phenomena.

Initial microcrack growth may arrest prior to and without the establishment of crack propagation conditions.

Initial surface conditions and associated immediate subsurface alloy microstructure layers generated during creation (i.e. disturbed layers) can dictate whether or not EIC initiation occurs under mechanical loading conditions sufficient to enable initiation and growth.

Allowance of sufficient primary creep exhaustion ahead of introduction of an aggressive environment can prevent EIC initiation, despite the mechanical driving force being well above conventional threshold (σ_{IEC} or K_{IEIC}) requirements.

Time-dependent local strain accommodation processes are important during EIC initiation at temperatures below 0.4 T_m.

Significant advances in the understanding the initiation of EIC in structural metals are now possible with the development of a wide range of new characterisation techniques that are starting to make an impact on this complex.

Research ethics: Not applicable.

Author contributions: NJHH generated the initial text with figures, other than section 2.6 (JJL) and section 2.7 (TLB). GMS revised and edited the first draft of the manuscript. All authors contributed to the final review and editing. The authors have accepted responsibility for the entire content of this manuscript and approved its submission. Competing interests: The authors state no conflict of interest.

Research funding: JJL would like to acknowledge the Arthur P Armington Professorship at CWRU as well as ONR funding under: N00014-24-1-2165, N00014-21-1-2090, N00014-17-12573, and the NSF Engineering Research Center for Hybrid Autonomous Manufacturing Moving from Evolution to Revolution (ERC-HAMMER) under Award Number EEC-2133630. NJHH was self-funded.

Data availability: Publications referenced in this contribution paper are in the Public Domain. Data may be obtained on request from the corresponding author.

References

Abe, M., Ouchi, K., Asano, K., and Fujiwara, A. (1981). Environmental embrittlement of an Al-Zn-Mg alloy. J. Jpn. Inst. Met. 45: 1161–1169, (in Japanese).

Aboura, Y. and Moore, K.L. (2021). NanoSIMS analysis of hydrogen and deuterium in metallic alloys: artefacts and best practice. Appl. Surf. Sci. 557: 149736.

Ahn, T.M. (2021). Long-term initiation time for stress-corrosion cracking of alloy 600 with implications in stainless steel: review and analysis for nuclear application. Prog. Nucl. Energy 137: 103760.

Alavi, A. and Cottis, R.A. (1987). The determination of pH, potential and chloride concentrations in corroding crevices on 304 stainless steel and 7475 aluminum alloy. Corros. Sci. 27: 443–451.

Anderson, P. and Chou, P. (2019). Crack initiation in alloy 600 in PRW water. In: Jackson, J.H., Paraventi, D., and Wright, M. (Eds.), Proceedings of 18th international conference on environmental degradation of materials in nuclear power systems - water reactors, Vol. 1. TMS Springer, Cham, pp. 121–135.

Andrade,E.D.C.andRandall,R.F.(1949).Therehbindereffect.

Nature164:1127. Anita, T., Pujar, M.G., Shaikh, H., Dayal, R., and Khatak, H.S. (2006). Assessment of stress corrosion crack initiation and propagation in AISI type 316 stainless steel by electrochemical noise technique. Corros. Sci.

48: 2689–2710.

Arioka, K. (2015). 2014 WR Whitney Award Lecture: change in bonding strength at grain boundaries before long-term SCC initiation. Corrosion 71: 403–419.

Arioka, K. (2020). Role of cavity formation on long-term stress corrosion cracking initiation: a review. Corrosion 76: 142–175.

Arioka, K., Miyamoto, T., Yamada, T., and Aoki, M. (2013). Role of cavity formation in crack initiation of cold-worked carbon steel in hightemperature water. Corrosion 69: 487–496.

Arioka, K., Miyamoto, T., Yamada, T., and Terachi, T. (2010). Formation of cavities prior to crack initiation and growth on cold-worked carbon steel in high-temperature water. Corrosion 66: 015008-015008.

Arioka, K., Yamada, T., Terachi, T., and Chiba, G. (2007). Cold work and temperature dependence of stress corrosion crack growth of

austenitic stainless steels in hydrogenated and oxygenated hightemperature water. Corrosion 63: 1114–1123.

Bakish, R. and Robertson, W.D. (1956a). Structure-dependent chemical reaction and nucleation of fracture in Cu_3Au single crystals. Acta Metall. 4: 342–351.

Bakish, R. and Robertson, W.D. (1956b). Structure dependent chemical activity of polycrystalline Cu_3Au-experiments relating to the mechanism of stress-corrosion cracking of homogeneous solid solutions. JOM 8: 1277–1282.

Barlow, P.L. (1966). Rehbinder effect in lubricated metal cutting. Nature 211:
1076–1077.

Beilby, G. (1921). Aggregation and flow of solids, 1st ed. Macmillan and Co, London.

Biserova-Tahchieva, A., Biezma-Moraleda, M.V., Llorca-Isern, N., GonzalezLavin, J., and Linhardt, P. (2023). Additive manufacturing processes in selected corrosion resistant materials: a state of knowledge review.
Materials 16: 1893.

Blanc, C., and Aubert, I. (Eds.) (2019). Mechanics-microstructure-corrosion coupling: concepts, experiments, modeling and cases. Elsevier, Oxford.

Blanc, C., Creus, J., and Touzet-Cotina, M. (2019) Stress corrosion cracking, between the corrosion defect and long crack: the phase of the initiation of the cracks (chapter 13). In: Blanc, C., and Aubert, I. (Eds.), Mechanics-microstructure-corrosion coupling: concepts, experiments, modeling and cases. Elsevier, Oxford, pp. 287–312.

Blanc, C. and Oltra, R. (2023). Environment-assisted crack initiation in aluminum alloys studied by local probe techniques. Corrosion 79: 17–34.

Bleckmann, I. and Zitter, H. (1974). Inkubationszeit und Rißverlauf bei der transkristallinen Spannungrißkorrosion austenitischer Chrom-NickelStähle in Magnesiumchlorid-Lösungen. Mater. Corros. 25: 93–97, (In German).

Bogdanov, R.I., Gutman, E.M., Ryakhovskikh, I.V., and Shneck, R.Z. (2019). Stress corrosion cracking of pipeline steels in near-neutral-pH solutions: the role of mechanochemical and chemomechanical effects. Вестигазовойнауки 40: 6–21.

Borchers, H. and Tenckhoff, E. (1969). Stress-corrosion cracking behaviour of aluminium-zinc-magnesium castings. Werkstoffe Korrosion 20: 319–323.

Boursier, J.M., Bouvier, O.D., Gras, J.M., Noel, D., Vaillant, F., and Rios, R. (1992). Stress corrosion cracking of alloy 600 in high temperature water: a study of mechanisms, Technical Report no. EDF—93-NB-00051.
Electricite de France (EDF), Paris.

Boursier, J.M., Desjardins, D., and Vaillant, F. (1995). The influence of the strain-rate on the stresscorrosion cracking of Alloy 600 in high temperature primary water. Corros. Sci. 37: 493–508.

Brauns, E. and Ternes, H. (1968). Untersuchungen über die transkristalline Spannungsrißkorrosion austenitischer Chrom-Nickel-Stähle in heißen Chloridlösungen. Werkstoffe und Korros 19: 1–19, (In German). (Investigations on the transcrystalline stress corrosion cracking of austenitic chromium-nickel steels in hot chloride solutions).

Brown, B.F. and Beachem, C.D. (1965). A study of the stress factor in corrosion cracking by use of the pre-cracked cantilever beam specimen. Corros. Sci. 5: 745–750.

Brown, B.F., Fujii, C.T., and Dahlberg, E.P. (1969). Methods for studying the solution chemistry within stress corrosion cracks. J. Electrochem. Soc.
116: 218–219.

Bruemmer, S.M. and Thomas, L.E. (2008) Insights into stress corrosion cracking mechanisms from high-resolution measurements of cracktip structures and compositions. In: Shipilov, S.A., Jones, R.H., and Olive, J.–m. (Eds.), Environment-induced cracking of materials, Vol. 2.
Elsevier, Oxford, pp. 95–106.

Burnett, T.L., Euesden, R.T., Aboura, Y., Yao, Y., Curd, M.E., Grant, C., Garner, A.J., Holroyd, N.J.H., Prangnell, P.B., Engel, C.E., et al. (2023). Mechanisms of environmentally induced crack initiation in humid air for new generation Al-Zn-Mg-Cu alloys. Corrosion 79: 850–886.

Burnett, T.L. and Withers, P.J. (2019). Completing the picture through correlative characterization. Nat. Mater. 18: 1041–1049.

Cassagne, T.B., Flanagan, W.F., and Lichter, B.D. (1986). On the failure mechanism of chemically embrittled Cu 3 Au single crystals. Metall. Trans. A 17: 703–710.

Chang, L., Burkes, M.G., and Scenini, F. (2019). Understanding effect of surface finish on stress corrosion crack initiation in warm-forged stainless steel 304L in high-temperature water. Scr. Mater. 164: 1–5.

Chen, W. (2017) Modeling and prediction of stress corrosion cracking of pipeline steels (chapter 30). In: El-Sherik, A.M. (Ed.). Trends in oil and gas corrosion research and technologies. Elsevier, Oxford, pp. 707–748.

Cocks, F.H., Russo, J.F., and Brummer, S.B. (1959). Separation of corrosion and stress effects in stress corrosion: the critical role of surface preparation. Corrosion 25: 345–349.

Coleman, E.G., Weinstein, D., and Rostoker, W. (1961). On a surface energy mechanism for stress-corrosion cracking. Acta Metallurgica 9:
491–496.

Colwell, J.A., Leis, B.N., and Singh, P.M. (2008) Crack initiation of line pipe steels in near-neutral pH environments. In: Environment-induced cracking of materials. Elsevier, Oxford, pp. 233–242.

Combrade, P. (2019). Environmentally assisted cracking: some critical aspects (chapter 1). In: Blanc, C., Aubert, I. (Eds). In: Mechanicsmicrostructure-corrosion coupling: concepts, experiments, modeling and cases. Elsevier, Oxford, pp. 1–22.

Connolly, B.J., Scully, J.R. (2000). Stress assisted pit and fissure coalescence during early stages of stress corrosion cracking in Al-Li-Cu alloy AA2096. In: CORROSION 2000 (NACE-00367). NACE, Houston, TX, pp.
<<<.

Cooper, K.R. and Kelly, R.G. (2007). Crack tip chemistry and electrochemistry of environmental cracks in AA 7050. Corros. Sci. 49: 2636–2662.

Cooper, K.R. and Kelly, R.G. (2008) Measurement and modeling of crack conditions during the environment-assisted cracking of an Al–Zn–Mg–Cu Alloy. In: Shipilov, S.A. (Ed.). Environmentally induced cracking of materials II. Elsevier, Oxford, pp. 335–344.

Crane, C.B. and Gangloff, R.F. (2016). Stress corrosion cracking of Al-Mg alloy 5083 sensitized at low temperature. Corrosion 72: 221–241.

Davis, J.A. (1971a). Use of microelectrodes for study of stress corrosion of aluminum alloys. In: Localized corrosion, Vol. 3. NACE, Houston, TX, pp. 168–172.

Davis, J.A. (1971b) pH and potential measurements during stress corrosion of aluminum alloy. In: AGARD (NATO) conference proceedings no. 48, specialist meeting on stress corrosion testing methods. Neuilly sur Seine and NATO (North Atlantic Treaty Organization), France.

Desjardins, D., Daret, J., Petit, M.C., and Pauthe, J.J. (1980). The correlation between mechanical and electrochemical parameters of stress corrosion cracking of austenitic stainless steels. Corros. Sci. 20: 177–187.

Eckel, J.F. (1962). Stress corrosion crack nucleation and growth in austenitic stainless steels. Corrosion 18: 270–276.

Economy, G., Jacko, R.J., and Pement, F.W. (1987). IGSCC behavior of alloy 600 steam generator tubing in water or steam above 360 ˚C. Corrosion 72: 727–734.

Edeleanu, C. and Evans, U.R. (1951). The causes of the localized character of corrosion on aluminium. Trans. Faraday Soc. 1947: 1121–1135.

Edwards, R.A.H. (1990). A simple mass-transport analysis of localized corrosion. In: Isaacs, H.S., Bertocci, U., Kruger, J., and Smialowska, S. (Eds.), Advances in localized corrosion (NACE 9). NACE, Houston, TX, pp. 381–392.

Elboujdaini, M., Wang, Y.Z., Wang, R.Y.Z., Revie, W., Shehata, M.T., Parkins, R.N. (2000). Stress corrosion crack initiation processes: pitting and microcrack coalescence. In: Corrosion 2000 (NACE-00379). NACE, Houston, TX.

Etien, R.A., Richey, E., Morton, D.S., and Eager, J. (2011) SCC initiation testing of alloy 600 in high temperature water. In: Proceedings of 15th international conference on environmental degradation of materials in nuclear power systems reactions. Wiley, New York, pp. 2407–2417.

Euesden, R.T., Aboura, Y., Garner, A.J., Jailin, T., Grant, C., Barrett, Z., Engel, C., Shanthraj, P., Holroyd, N.J.H., Prangnell, P.B., et al. (2023). In-situ observation of environmentally assisted crack initiation and short
crack growth behavior of New-Generation 7xxx series aluminum alloys in humid air. Corros. Sci. 216: 111051.

Fairweather, N.D., Platts, N., Tice, D.R. (2008). Stress-corrosion crack initiation of type 304 stainless steel in atmospheric environments containing chloride: influence of surface condition, relative humidity, temperature and thermal sensitization. In: Corrosion 2008 (NACE08485). NACE, Houston, TX.

Forsyth, P.J.E. (1998). Sequence of corrosion attack of machining induced flow zone produced on some Al alloys that leads to rapid intergranular penetration. Mater. Sci. Technol. 14: 151–160.

Forty, A.J. (1959) The initiation and propagation of cracks in the stress corrosion of αbrass and similar alloys. In: Rhodin, T.N. (Ed.). Physical metallurgy of stress corrosion fracture. Interscience Publishers, Inc, New York, pp. 99–115.

Fujii, T., Tohgo, K., Mori, Y., Miura, Y., and Shimamura, Y. (2019). Crystallographic and mechanical investigation of intergranular stress corrosion crack initiation in austenitic stainless steel. Mater. Sci. Eng., A 751: 160–170.

Gault, B., Moody, M.P., Cairney, J.M., and Ringer, S.P. (2012). Atom probe microscopy 2012, Vol. 160. Springer Science & Business Media, New York.

Gooch, D.J. (1984). The effect of cold work on low temperature (0.35 Tm) creep crack growth in C-Mn steels. Mater. Sci. Eng. 64: 183–196.

Griesche,A., Eitan, D., Kannengiesser, T., Kardjilov, N., Hilger, A., and Manke, I. (2014). Three-dimensional imaging of hydrogen blister in iron with neutron tomography. Acta Mater. 78: 14–22.

Gu, B., Qiao, L.J., Ghu, W.Y., and Hsiao, C.M. (1994). The effect of pre-creep on stress corrosion cracking of austenitic stainless steel and brass.
Corros. Sci. 36: 1447–1455.

Gudla, V.C., Storm, M., Palmer, B.C., Lewandowski, J.J., Withers, P.J., Holroyd, N.J.H., and Burnett, T.L. (2020). Environmentally induced crack (EIC) initiation, propagation, and failure: a 3D in-situ time-lapse study of AA5083 H131. Corros. Sci. 174: 108834.

Gutierrez-Urrutia, I., Zaefferer, S., and Raabe, D. (2013). Coupling of electron channeling with EBSD: toward the quantitative characterization of deformation structures in the SEM. JOM 65: 1229–1236.

Gutman, E.M., Solovioff, G., and Eliezer, D. (1996). The mechanochemical behavior of type 316L stainless steel. Corros. Sci. 38: 1141–1145.

Harris, Z.D., Dolph, J.D., Pioszak, G.L., Troconis-Rincon, B.C., Scully, J.R., and Burns, J.T. (2016). The effect of microstructural variation on the hydrogen environment-assisted cracking of Monel K-500. Metall. Mater. Trans. A 47: 3488–3510.

Harwood, J.J. (1956) The phenomena and mechanism of stress corrosion cracking. In: Robertson, W.D. (Ed.). Stress corrosion cracking and embrittlement. John Wiley & Son, Inc., New York, pp. 11–20.

Harwood, J.J. (1960). The mechanism of stress-corrosion cracking of austenitic stainless steels. In: Rogers, l. (Ed.). Report on stress-corrosion cracking of austenitic chromium-nickel stainless steels. ASTM-STP 48323S, West Conshohocken, PA, pp. 22–23, 63–67.

Henthorne, M. (2016). The slow strain rate stress corrosion cracking test – a 50-year retrospective. Corrosion 72: 1488–1518.

Hickling, J., Taylor, D.F., and Andresen, P.L. (1998). Use of electrochemical noise to detect stress corrosion crack initiation in simulated BWR environments. Mater. Corros. 49: 651–658.

Hilfrich, W.J. (1968). Development of a rapid stress-corrosion test for aluminum alloys, NASA final summary report. Contract no. NAS8-20285. Kaiser Alumium and Chemicals Corportation, Pleaston, CA.

Hines, J.G. (1961). The development of stress corrosion cracking in austenitic Cr-Ni steels. Corros. Sci. 1: 2–20.

Hirth, J.P. (1977) SCC and HE from the view point of the defect solid state. In:
Staehle, R.W., Hochmann, J., McCright, R.D., Slater, J.E., and Housten (Eds.), Stress corrosion cracking and hydrogen embrittlement of iron based alloys. NACE-5, Houston, TX, pp. 1–10.

Hoar, T.P. and Hines, J.D. (1954). The corrosion potential of stainless steels during stress corrosion. J. Iron Steel Inst. 177: 248.

Hoar, T.P. and Hines, J.D. (1956a). The stress-corrosion cracking of austenitic steels – Part 1: mechanism and process in hot magnesium chloride solutions. J. Iron Steel Inst. 182: 124–143.

Hoar, T.P. and Hines, J.D. (1956b). The stress-corrosion cracking of austenitic steels – Part 2: fully softened, strain-hardened and refrigerated material. J. Iron Steel Inst. 184: 166–172.

Hojna, A. (2021). Environmentally assisted cracking initiation in hightemperature water. Metals 11: 199.

Holroyd, N.J.H., Burnett, T.L., Lewandowski, J.J., and Scamans, G.M. (2023). Environment-induced crack initiation in aluminum alloys: experimental studiessince the1950's and future opportunities.Corrosion79:850–866.

Holroyd, N.J.H., Evans, J.T., and Scamans, G.M. (2015). Pre-exposure embrittlementofanAl-Cu-Mgalloy,AA2024-T351.Corros.Rev.33:361–372.

Holroyd, N.J.H., Scamans, G.M., and Hermann, R. (1984) Environmental interaction with the crack tip region during environment sensitive fracture of aluminum alloys. In: Gangloff, R.P. (Ed.). Embrittlement by the localized crack environment. TMS/AIME, New York, pp. 327–347.

Holroyd, N.J.H., Scamans, G.M., and Hermann, R. (1987) Environmental conditions within crevices and stress corrosion cracks in aluminum alloys. In: Turnbull, A. (Ed.). Corrosion chemistry within pits, crevices and cracks. Her Majesty's Stationery Office, UK, pp. 495–510.

Horner, D.A., Connolly, B.J., Zhou, S., Crocker, L., and Turnbull, A. (2011). Novel images of the evolution of stress corrosion cracks from corrosion pits. Corros. Sci. 53: 3466–3485.

Hunter, M.S. and Fickle, W.G. (1968). Study of crack initiation phenomena associated with stress corrosion of aluminum alloys, 2nd annual report. In: Contract no. NAS 8-20285. ALCOA (Aluminum Company of America), New Kensington, PA.

Isaacs, H.S. (1988). Initiation of stress corrosion cracking of sensitized type 304 stainless steel in dilute thiosulfate solution. J. Electrochem. Soc. 135: 2180–2183.

Jones,R.H.,Friese,IM.A.,and Pathania,R.(1991).Evaluation ofstress corrosion crack initiation using acoustic emission. Corrosion 47: 105–115.

Jones, R.H. and Simonen, E.P. (1994). Early stages in the development of stress corrosion cracks. Mater. Sci. Eng. A176: 211–218.

Kamaya, M. and Takumi, H. (2007). Influence of local stress on initiation behavior of stress corrosion cracking for sensitized 304 stainless steel.
Corros. Sci. 49: 3303–3324.

Katona, R.M., Karasz, E.K., and Schaller, R.A. (2023). Review of the governing factors in pit-to-crack transitions of metallic structures. Corrosion 79:
72–96.

Kelly, R.G. (2021). 2021 W.R. Whitney Award: the importance of local chemistry and potential in localized corrosion and stress corrosion cracking. Corrosion 78: 114–126.

Kim, K., Ahn, G., and Kim, S.W. Song. (2023). Combinationof X-ray diffraction and X-ray scattering and spectroscopy. Corros. Sci. 218: 111176.

Kim, S., Ahn, K., Kim, G., and Song, S.W. (2023). Synchrotron X-ray fluorescence imaging study on chloride-induced stress corrosion cracking behavior of austenitic stainless steel welds via selective corrosion of δ-ferrite. Corros. Sci. 218: 111176.

King, A., Johnson, G., Engelberg, D., Ludwig, W., and Marrow, T.J. (2008). Observations of intergranular stress corrosion cracking in a grainmapped polycrystal. Science 321: 382–385.

Kirk, W.W., Beck, F.H., and Fontana, M.G. (1959) Stress corrosion cracking of austenitic steels in high temperature chloride waters. In: Rhodin, T.N. (Ed.). Physical metallurgy of stress corrosion fracture. Interscience Publishers, New York, pp. 227–246.

Kohl, H. (1967). A contribution to the examination of stress corrosion cracking of austenitic stainless steels in magnesium chloride solutions. Corrosion 23: 39–49.

Koko, A., Singh, S., Barhli, S., Connolley, T., Vo, N.T., Wigger, T., Liu, D., Fu, Y., Réthoré, J., Lechambre, J., et al. (2023). 3-Dimensional analysis of fatigue crack fields and crack growth by in situ synchrotron X-ray tomography. Int. J. Fatig. 170: 107541.

Komai, K., Minoshima, K., and Miyawaki, T. (1988). In situ observation of stress corrosion cracking of high-strength aluminum alloy by scanning atomic force microscopy and influence of vacuum. JSME Int. J. Ser. A Solid Mech. Mater. Eng. 41: 49–56.

Koyama, M., Rohwerder, M., Tasan, C.C., Bashir, A., Akiyama, E., Takai, K., Raabe, D., and Tsuzaki, K. (2017). Recent progress in microstructural hydrogen mapping in steels: quantification, kinetic analysis, and multi-scale characterization. Mater. Sci. Technol. 33: 1481–1496.

Kuang, W. and Was, G.S. (2000). A high-resolution characterization of the initiation of stress corrosion crack in Alloy 690 in simulated pressurized water reactor primary water. Corros. Sci. 163: 108243.

Kujawski, D. and Krempl, E. (1981). The rate (time)-dependent behavior of Ti7Al-2Cb-1Ta titanium alloy at room temperature under quasi-stic monotonic and cyclic loading. J. Appl. Mech. 48: 55–63.

Kumar, A.N. (2008) Susceptibility to and the mechanism of stress-corrosion cracking in structural steels in aqueous solutions. In: Environmentinduced cracking of materials. Elsevier, Oxford, pp. 395–404.

Kwon, H.S., Hehemann, R.F., and Troiano, A.R. (1992). Critical cracking potentials of 26Cr-1 Mo ferritic steels in boiling 42% LiCl solution. Corrosion 48: 838–845.

Leckie, H.P. (1967). Stress corrosion characteristics of a Ti-7Al-2Cb-1Ta alloy. Corrosion 23: 187–191.

Lee, S.M., Kim, K.T., and Pyun, S. (1988). Kinetics of intergranular corrosion and separation between initiation and propagation of stress corrosion crack in mild steel. Scripta Met 22: 31–34.

Lees, D.J. and Siverns, M.J. (1978) Preventing failures in boiler feeder pipes carrying steam. In: Tolerance of flaws in pressurized components. Institution of Mechanical Engineers, London, pp. 193–204.

Le Hong, S. (2001). Influence of surface condition on primary water stress corrosion cracking initiation of alloy 600. Corrosion 57: 323–333.

Lewandowski, J.J. and Seifi, M. (2016). Additive manufactured metals: a review of mechanical properties. ARMR paper. Annu. Rev. Mater. Res.: 151–186, https://doi.org/10.1146/annurev-matsci-070115-032024.

Li, K., Liu, J., Grovenor, C.R.M., and Moore, K.L. (2020). NanoSIMS imaging and analysis in materials science. Annu. Rev. Anal. Chem. 13: 273–292.

Liu, X., Frankel, G.S., Zoofan, B., and Rokhlin, S.I. (2004). Effect of applied tensile stress on intergranular corrosion of AA2024-T3. Corros. Sci. 46: 405–425.

Liu, X., Frankel, G.S., Zoofan, B., and Rokhlin, S.I. (2007). In-situ observation of intergranular stress corrosion cracking in AA2024-T3 under constant load conditions. Corros. Sci. 49: 139–148.

Locci, I.E., Kwon, H.K., Hehemann, R.F., and Trioiano, A.R. (1987). Stress corrosion cracking initiation in ferritic stainless steels in a chloride environment. Corrosion 43: 465–470.

Logan, H.L. (1961). Stress corrosion cracking of the AZ31B magnesium alloy. J. Res. Nat. Bur. Stand. C 65: 165–169.

Louthan, M.R. (1965). Initial stages of stress corrosion cracking in austenitic stainless steels. Corrosion 21: 288–294.

Lozano-Perez, S., Dohr, J., Meisnar, M., and Kruska, K. (2014). SCC in PWRs: learning from a bottom-up approach. Metall. Mater. Trans. E 1: 194–210.

Lynch, S.P. (1977) Mechanism of liquid-metal embrittlement and stresscorrosion cracking on high-strength aluminum alloys and other materials. In: Swann, P.R., Ford, F.P., and Westwood, A.R.C. (Eds.), Mechanism of environment sensitive cracking of materials. The Metals Society, London, pp. 201–212.

Lynch, S.P. (1988). Environmentally assisted cracking: overview of evidence for an adsorption-induced localized-slip process. Acta Metall. 36:
2639–2661.

Lynch, S.P. (2013). Mechanisms and kinetics of environmentally assisted cracking: current status, issues, and suggestions for further work. Metall. Mater. Trans. A 44: 1209–1229.

Ma, Z., Xiong, X., Chen, L., and Su, Y. (2021). Quantitative calibration of the relationship between Volta potential measured by scanning Kelvin probe force microscope (SKPFM) and hydrogen concentration.
Electrochim. Acta 366: 137422.

Magdowski, R.M. (1987). Stress corrosion cracking of low alloy steel in water, Doctoral dissertation. ETH, Zurich.

Maire, E. and Withers, P.J. (2014). Quantitative X-ray tomography. Int. Mater. Rev. 59: 1–43.

Maiya, P.S. (1989). Plastic strain, environmental, and crevice effects on SCC initiation and propagation in types 316NG and 304 stainless steel.
Corrosion 45: 915–924.

McCarroll, E., Bagot, P.A.J., Devaraj, A., Perea, D.E., and Cairney, J.M. (2000). New frontiers in atom probe tomography: a review of research enabled by cryo and/or vacuum transfer systems. Mater. Today Adv.
2000: 100090.

McHardy, J. and Hollingsworth, E.H. (1966). Investigation of the mechanism of stress corrosion of aluminum alloys, Final Report, US Navy, Bureau of Naval Weapons. Contract Now 65-0327-f, ALCOA (Aluminum Company of America), New Kensington, PA.

Moss, T. and Was, G.S. (2017). Accelerated stress corrosion crack initiation of alloys 600 and 690 in hydrogenated supercritical water. Metall. Mater. Trans. A 48A: 1613–1628.

Moss, T. and Was, G.W. (2013). Accelerated stress corrosion crack initiation of Alloy 690 and Alloy 600 in high temperature hydrogenated water. In: 16th International conference on environmental degradation of materials in nuclear power system-water reactors, Asheville, NC, pp. <<<.

Novak, S.R. and Wolfe, S.T. (1970). Comparison of fracture mechanics and nominalstressanalyses instresscorrosioncracking.Corrosion26:121–130.

Örnek, C., Zhang, F., Larsson, A., Mansoor, M., Harlow, G.S., Kroll, R., Carlà, R.F., Hussain, H., Engelberg, D.L., Derin, B., et al. (2023). Understanding passive film degradation and its effect on hydrogen embrittlement of super duplex stainless steel–Synchrotron X-ray and electrochemical measurements combined with CalPhaD and ab-initio computational studies. Appl. Surf. Sci. 628: 157364.

Parkins, R.N. (1977). Environmental aspects of stress corrosion cracking in low strength ferritic steels. In: Staehle, R.W., Hochmann, J., McCright, R.D., and Slater, J.E. (Eds.), Conference proceedings of NACE-5, stress corrosion cracking and hydrogen embrittlement of iron based alloys. NACE, Houston, TX, pp. 601–624.

Parkins, R.N. (1979) Development of strain-rate testing and its implications. In: Ugiansky, G.M., and Payer, J.H. (Eds.), The slow strain rate technique. ASTM STP665, West Conshohocken, PA, pp. 5–25.

Parkins, R.N. (1988). Localized corrosion and crack initiation. Mater. Sci. Eng.
A 103: 143–156.

Parkins, R.N. and Greenwell, B.S. (1977). The interface between corrosion fatigue and stress-corrosion cracking. Metal Sci. 1: 405–413.

Parkins, R.N. and Singh, P.M. (1990). Stress corrosion crack coalescence. Corrosion 46: 485–499.

Pathania, R.S. (1970). Stress corrosion cracking of aluminum alloys, PhD thesis. University of British Columbia, Vancouver.

Pathania, R.S. and Tromans, D. (1981). Initiation of stress corrosion cracks in aluminum alloys. Metall. Trans. A 12: 607–612.

Paxton, H.W. and Procter, R.P.M. (1968). The effects of machining and grinding on the stress-corrosion cracking of metals and alloys, Final Report EM68-520 (AD 684875). American Society of Tool and Manufacturing Engineers, Dearborn, MI.

Persaud, S.Y., Smith, J.M., and Newman, R.C. (2019). Nanoscale precursor sites and their importance in the prediction of stress corrosion cracking failure. Corrosion 75: 228–239.

Petit, M.C. and Desjardins, D. (1977) Elongation measurements of stainless steel during SCC tests. In: Staehle, R.W., Hochmann, J., McCright, R.D., and Slater, J.E. (Eds.), Conference proceedings of NACE-5, stress corrosion cracking and hydrogen embrittlement of iron based alloys, Houston, TX, pp. 1205–1210.

Pickering, H.W. and Swann, P.R. (1963). Electron metallography of chemical attack upon some alloys susceptible to stress corrosion cracking.
Corrosion 19: 373t–389t.

Pugh, E.N. (1971) The mechanism of stress corrosion cracking of alpha-brass in aqueous ammonia. In: Scully, J.C. (Ed.). The theory of stress corrosion cracking in alloys. NATO, Brussels, pp. 418–441.

Rebak, R.B. and Lou, X. (2018). Environmental cracking and irradiation resistant stainless steels by additive manufacturing, No. NE0008428.
General Electric Co., Schenectady, NY, USA.

Rehbinder, P. (1947). New physico-chemical phenomena in the deformation and mechanical treatment of solids. Nature 159: 866–867.

Richey, E., Morton, D.S., Etien, R.A. (2007). SCC initiation testing of nickelbased alloys in high temperature water. In: Proceedings of 13th international conference on environmental degradation of

materials in nuclear power systems reactions, Canadian Nuclear Society, Whistler, BC, p. 831.

Rieck, R.M., Atrens, A., and Smith, I.O. (1989). The role of crack tip strain rate in the stress corrosion cracking of high strength steels in water. Met. Trans. A 20A: 889–895.

Rios, R., Magnin, T., Noel, D., and De Bouvier, O. (1995). Critical analysis of alloy 600 stress corrosion cracking mechanisms in primary water. Metall. Mater. Trans. A 26: 925–939.

Roberts-Austen, W.C. (1888). On certain mechanical properties of in metals considered in relation to the Periodic Law. Philos. Trans. R. Soc. London A179: 339–350.

Sandoz, G., Fujii, C.T., and Brown, B.F. (1970). Solution chemistry within stress-corrosion cracks in steels. Corros. Sci. 10: 839–845.

Santamaria, R., Wang, K., Salasi, M., Selem, M., Lours, P., Iannuzzi, M., and Quadir, M.Z. (2023). Stress corrosion cracking behavior of austenitic stainless steel 316L produced using laser-based powder bed fusion.
Corrosion 79: 944–955.

Scamans, G.M., Frolish, M.F., Rainforth, W.M., Zhou, Z., Liu, Y., Zhou, X., and Thompson, G.E. (2010). The ubiquitous Beilby layer on aluminium surfaces. Surf. Interface Anal. 42: 175–179.

Scenini, F., Lindsay, J., Chang, L., Wanyg, Y.L., Burke, M.G., Lozano-Perez, S., Pimentel, G., Tice, D., Mottershead, K., and Addepalli, V. (2019). Oxidation and SCC initiation studies of 304L SS in PWR primary water. In: Jackson, J.H., Paraventi, D., and Wright, M. (Eds.), Proceedings of the 18th international Conference on environmental Degradation of Materials in nuclear power systems - water reactors, Vol. 1. Springer International Publishing, Cham, pp. 793–810.

Schra, L. and Wanhill, R.J.H. (1997). Evaluation of ASCOR test method for stress corrosion testing of aluminum alloys. In: National Aerospace Laboratory Report NLR-TR, 97392. National Aerospace Laboratory, Amsterdam, The Netherlands.

Schra, L. and Wanhill, R.J.H. (1999). Further evaluation of automated stress corrosion ring (ASCOR) testing of aluminum alloys. J. Test Eval. 27:
196–201.

Shen, Z., Roberts, E., Saravanan, N., Karamched, P., Terachi, T., Yamada, T., Wu, S., Tarleton, E., Armstrong, D.E.J., Withers, P.J., et al. (2022). On the role of intergranular nanocavities in long-term stress corrosion cracking of alloy 690. Acta Mater. 222: 117453.

Shi, Hui-Ji., Ruan, C., and Li, X. (2006). Study of the initiation stage of stress corrosion of an aluminum alloy using the subjective speckle technique. Mater. Sci. Eng. A 419: 218–224.

Sieradzki, K., Kimm, J.M., Cole, A.T., and Newman, R.C. (1987). The relationship between dealloying and transgranular stress-corrosion cracking of Cu-Zn alloys. J. Electrochem. Soc. 137: 1635–1639.

Silcock, J.M. and Swann, P.R. (1977) Microstructural aspects of environmental sensitive failure of austenitic stainless steels. In: Swann, P.R., Ford, F.P., and Westwood, A.R.C. (Eds.), Mechanism of environment sensitive cracking of materials. The Metals Society, London, pp. 66–52.

Singh, S.S., Williams, J.J., Lin, M.F., Xiao, X., Carlo, F.D., and Chawla, N. (2014). In situ investigation of high humidity stress corrosion cracking of 7075 aluminum alloy by three-dimensional (3D) X-ray synchrotron tomography. Mater. Res. Lett. 2: 217–220.

Sircar, S.C. and Narsaria, S.K. (1977). On separation of initiation and propagation stages in stress corrosion cracking of alpha brass. Corros. Sci. 17: 615–624.

Smialowski, M. and Kostanski, J. (1979). Creep and stress corrosion cracking of austenitic stainless steel in boiling 35% magnesium chloride solution. Corros. Sci. 19: 1019–1029.

Smith, T.J. and Staehle, R.W. (1967). Role of slip step emergence in the early stages of stress corrosion cracking in face centered iron-nickelchromium alloys. Corrosion 23: 117–129.

Staehle, R.W. (2008) Predicting failures in light water nuclear reactors which have not yet been observed: microprocess sequence approach (MPSA). In: Environment-induced cracking of materials. Elsevier, Oxford, pp. 3–54. Staehle, R.W. (2010). Critical analysis of “tight cracks”. Corros. Rev. 28: 1–103.

Sugimoto, K., Takahashi, K.I., and Sawada, Y. (1978). Induction and propagation periods during stress-corrosion cracking of 18–8 stainless steel in concentrated MgCl2 solutions. Trans. Jpn. Inst. Metal.
19: 422–430.

Swann, P.R. (1963). Dislocation substructure vs transgranular stress corrosion susceptibility of single phase alloys. Corrosion 19: 102–112.

Szklarska-Smialowska, Z. and Gust, J. (1979). The initiation of stress corrosion cracks and pits in austenitic CrNi steel in MgCl2 solutions at 40–90° C. Corros. Sci. 19: 753–766.

Taylor, M., Smith, A.D., Donoghue, J.M., Burnett, T.L., and Pickering, E.J. (2024). In-situ heating-stage EBSD validation of algorithms for prioraustenite grain reconstruction in steel. Scr. Mater. 242: 115924.

Tromans, D. and Nutting, J. (1962) Electron microscope studies of stress corrosion cracking. In: Fracture of solids. Interscience Publishers, New York, pp. 637–655.

Turnbull, A. (1990). Chemistry within localized corrosion cavities. In: Isaacs, H.S., Bertocci, U., Kruger, J., and Smialowska, S. (Eds.), Advances in localized corrosion (NACE 9). NACE, Houston, TX, pp. 359–373.

Turnbull, A. (1993). Modelling of environment assisted cracking. Corros. Sci. 34: 941–960.

Turnbull, A. (2001). Modelling of the chemistry and electrochemistry in cracks – a review. Corrosion 57: 175–189.

Turnbull, A. (2017). Characterising the early stages of crack development in environment-assisted cracking. Corros. Eng., Sci. Technol. 52: 533–540.

Turnbull, A. (2021). Reflections on early stages of environmentally assisted cracking from corrosion pits. Corros. Mater. Degrad. 2: 568–581.

Turnbull, A., Horner, D.A., and Connolly, B.J. (2009). Challenges in modelling the evolution of stress corrosion cracks from pits. Eng. Fract. Mech. 76:
633–640.

Turnbull, A. and Zhou, S. (2004). Pit to crack transition in stress corrosion cracking of a steam turbine disc steel. Corros. Sci. 46: 1239–1264.

Ugiansky, G.M. and Payer, J.H. (1979) Introduction. In: Ugiansky, G.M., and Payer, J.H. (Eds.), Stress corrosion cracking – the slow strain rate technique. ASTM STP 665, Philadelphia, PA, pp. 1–2.

Uhlig, H.H. (1959) New perspectives in the stress corrosion problem. In: Physical metallurgy of stress corrosion cracking fracture. Interscience Publishers, New York, pp. 1–17.

Uhlig, H.H. (1977) Stress sorption cracking and the critical potential. In: Staehle, R.W., Hochmann, J., McCright, R.D., and Slater, J.E. (Eds.), Conference proceedings of NACE-5, stress corrosion cracking and hydrogen embrittlement of iron based alloys, Houston, TX, pp. 174–179.

Uhlig, H.H. and Cook, E.W. (1969). Mechanism of inhibiting stress corrosion cracking of 18-8 stainless steel in $MgCl_2$ by acetates and nitrates. J. Electrochem. Soc. 116: 173–177.

Volpe, L., Burke, M.G., and Scenini, F. (2020). Correlation between grain boundary migration and stress corrosion cracking of alloy 600 in hydrogenated steam. Acta Mater. 186: 454–466.

Wang, F., Stinville, J.C., Charpagne, M., McLean, P., Echlin, M.P., Agnew, S.R., Pollock, T.M., De Graef, M., and Gianola, D.S. (2023). Dislocation cells in additively manufactured metallic alloys characterized by electron backscatter diffraction pattern sharpness. Mater. Charact. 197: 112673.

Wang, Z.F. and Atrens, A. (1996). Initiation of stress corrosion cracking for pipeline steels in a carbonate-bicarbonate solution. Metall. Mater. Trans. A 27: 2686–2691.

Wearmouth, W.R., Dean, G.P., and Parkins, R.N. (1973). Role of stress in the stress corrosion cracking of a Mg-Al alloy. Corrosion 29: 251–258.

Wilde, B.E. (1969). Technique for studying the kinetics of intergranular crack nucleation on AISI type 304 stainless steel in oxygenated water at 289 C. Corrosion 25: 359–365.

Yan, J., Chen, T., Gutman, E.M., and Unigovski, Y.B. (2023). Kinetic nature of electrochemical plasticization. Int. J. Plast. 171: 103820.

Yang, L., He, L., Huang, D., Wang, Y., Song, Q., Zhao, L., Shen, X., Tian, Z., and Wang, H. (2020). Three-dimensional hydrogen distribution and quantitative determination of titanium alloys via neutron tomography. Analyst 145: 4156.

Yang, Y., Scenini, F., and Curioni, M. (2016). A study on magnesium corrosion by real-time imaging and electrochemical methods: relationship between local processes and hydrogen evolution. Electrochim. Acta 198: 174–184.

Yardley, S.S., Moore, K.L., Ni, N., Wei, J.F., Lyon, S., Preuss, M., Lozano-Perez, S., and Grovenor, C.R.M. (2013). An investigation of the oxidation behaviour of zirconium alloys using isotopic tracers and high resolution SIMS. J. Nucl. Mater. 443: 436–443.

Yavuzyegit, B., Avcu, E., Smith, A.D., Donoghue, J.M., Lunt, D., Robson, J.D., Burnett, T.L., da Fonseca, Q.J., and Withers, P.J. (2023). Mapping plastic deformation mechanisms in AZ31 magnesium alloy at the nanoscale. Acta Mater. 250: 118876.

Yazdanpanah, A., Franceschi, R.I., Khademzadeh, S., De Graeve, I., and Dabala, M. (2022). Revealing the stress corrosion cracking initiation mechanism of alloy 718 prepared by laser powder bed fusion assessed by microcapillary method. Corros. Sci. 208: 110642.

Yin, J. and Yuan, Q. (2023). Mechanism of crack evolution and strength failure in chemo-mechanical induced fracture. J. Mech. Phys. Solid. 183: 105525.

Yu, J., Holroyd, N.J.H., and Parkins, R.N. (1984) Application of slow-strain-rate tests to defining the stress for stress corrosion cracking in 70/30 brass. In: Dean, S.W., Pugh, E.N., and Ugiansky, G.M. (Eds.), Environmentsensitive fracture: evaluation and comparison of test methods. ASTM STP 821, Philadelphia, PA, pp. 288–309.

Zhai, Z., Toloczko, M., Kruska, K., and Bruemmer, S.M. (2017b). Precursor evolution and stress corrosion cracking initiation of cold-worked alloy 690 in simulated pressurized water reactor primary water. Corrosion 73: 1224–1236.

Zhai, Z., Toloczko, M.B., Kruska, K., and Olszta, K. (2017a). Bruemmer SM. Stress corrosion initiation of alloy 6000 I PWR primary water. Corros. Sci. 123: 76–87.

Zhao, H., Chakraborty, P., Ponge, D., Hickel, T., Sun, B., Wu, C.H., Gault, B., and Raabe, D. (2022). Hydrogen trapping and embrittlement in highstrength Al alloys. Nature 602: 437–441.